



HAL
open science

Rab11a–Rab8a cascade regulates the formation of tunneling nanotubes through vesicle recycling

Seng Zhu, Shaarvari Bhat, Sylvie Syan, Yoshihiko Kuchitsu, Mitsunori Fukuda, Chiara Zurzolo

► **To cite this version:**

Seng Zhu, Shaarvari Bhat, Sylvie Syan, Yoshihiko Kuchitsu, Mitsunori Fukuda, et al.. Rab11a–Rab8a cascade regulates the formation of tunneling nanotubes through vesicle recycling. *Journal of Cell Science*, 2018, 131 (19), pp.jcs215889. 10.1242/jcs.215889 . pasteur-02263630

HAL Id: pasteur-02263630

<https://pasteur.hal.science/pasteur-02263630>

Submitted on 5 Aug 2019

HAL is a multi-disciplinary open access archive for the deposit and dissemination of scientific research documents, whether they are published or not. The documents may come from teaching and research institutions in France or abroad, or from public or private research centers.

L'archive ouverte pluridisciplinaire **HAL**, est destinée au dépôt et à la diffusion de documents scientifiques de niveau recherche, publiés ou non, émanant des établissements d'enseignement et de recherche français ou étrangers, des laboratoires publics ou privés.

RESEARCH ARTICLE

Rab11a–Rab8a cascade regulates the formation of tunneling nanotubes through vesicle recycling

Seng Zhu^{1,*}, Shaarvari Bhat^{1,*}, Sylvie Syan¹, Yoshihiko Kuchitsu², Mitsunori Fukuda² and Chiara Zurzolo^{1,‡}

ABSTRACT

Tunneling nanotubes (TNTs) are actin-enriched membranous channels enabling cells to communicate over long distances. TNT-like structures form between various cell types and mediate the exchange of different cargos, such as ions, vesicles, organelles and pathogens; thus, they may play a role in physiological conditions and diseases (e.g. cancer and infection). TNTs also allow the intercellular passage of protein aggregates related to neurodegenerative diseases, thus propagating protein misfolding. Understanding the mechanism of TNT formation is mandatory in order to reveal the mechanism of disease propagation and to uncover their physiological function. Vesicular transport controlled by the small GTPases Rab11a and Rab8a can promote the formation of different plasma membrane protrusions (filopodia, cilia and neurites). Here, we report that inhibiting membrane recycling reduces the number of TNT-connected cells and that overexpression of Rab11a and Rab8a increases the number of TNT-connected cells and the propagation of vesicles between cells in co-culture. We demonstrate that these two Rab GTPases act in a cascade in which Rab11a activation of Rab8a is independent of Rabin8. We also show that VAMP3 acts downstream of Rab8a to regulate TNT formation.

KEY WORDS: Rab GTPase, Tunneling nanotube, Vesicle recycling, Vesicle transfer

INTRODUCTION

Tunneling nanotubes (TNTs) are thin membranous structures that connect distant cells. Observed in different cell types, TNTs are normally observed as straight membrane protrusions hovering above the substrate between two cells (Rustom et al., 2004). TNTs act as conduits between cells that allow the exchange of both cell-surface molecules and cytoplasmic content such as endosomes, mitochondria, endoplasmic reticulum and calcium ions (Abouinit and Zurzolo, 2012; Marzo et al., 2012). TNTs can also be hijacked by different pathogens, including prions (Gousset et al., 2009; Zhu et al., 2017), bacteria (Onfelt et al., 2006) and viruses (Kadiu and Gendelman, 2011; Sherer and Mothes, 2008; Sowinski et al., 2008), thus participating in the propagation of a wide range of diseases. Interestingly, several misfolded proteins associated with neurodegenerative diseases, such as β -amyloid (A β), tau, α -synuclein (α -syn) and huntingtin polyglutamine aggregates, have been found

inside TNTs, supporting the hypothesis that TNTs are a preferential highway for the spreading of proteinaceous aggregates (Abouinit et al., 2016a,b; Marzo et al., 2012; Victoria and Zurzolo, 2017; Wang et al., 2011).

TNTs principally comprise continuous actin filaments that are enclosed in a lipid bilayer (Austefjord et al., 2014). In some cells (e.g. macrophages), TNTs have been shown to also contain microtubules organized in bundles parallel to the major axis (Sanchez et al., 2017). The formation of TNTs can be impaired by the use of F-actin-depolymerizing drugs, such as latrunculin and cytochalasin D (Bukoreshtliev et al., 2009; Gousset et al., 2009; Rustom et al., 2004), suggesting that actin polymerization plays an important role in TNT formation. However, the mechanism underlying TNT formation is not completely understood and it is possible that different mechanisms are involved in different cell types (Abouinit and Zurzolo, 2012; Gousset et al., 2013).

Time-lapse imaging studies have previously suggested two possible mechanisms of TNT formation: (1) actin-driven protrusion outgrowth (Abouinit and Zurzolo, 2012; Reichert et al., 2016; Rustom et al., 2004) and (2) cell dislodgement (Davis and Sowinski, 2008; Rustom et al., 2004; Sowinski et al., 2008). Based on our current understanding, an intercellular bridge is established by the outgrowth of a filopodia-like protrusion containing F-actin from either one or both cells. After extension, the tip of the filopodia-like protrusion contacts the target cell directly (or through adhesion molecules) and could (or not) fuse with the receiving cell (Rustom et al., 2004). On the other hand, it has been proposed that when two cells come into physical contact with each other, they could either form an immune synapse (Dustin et al., 2010; Reichert et al., 2016) or fuse temporarily. After plasma membrane fusion, cells continue to migrate in opposing directions, stretching out the plasma membranes to form TNTs that could be formed by either one or two cells. Although the first mechanism is more common in immobile cells such as neurons, the latter is mainly found in motile cells such as macrophages and other cells of the immune system (Abouinit and Zurzolo, 2012).

Several proteins controlling actin polymerization and depolymerization have been shown to play a role in filopodia formation. Among these proteins, the cell division control protein 42 homolog (CDC42), a small GTPase of the Ras superfamily, regulates actin polymerization through direct binding to the neural Wiskott–Aldrich syndrome protein (N-WASP), which subsequently activates Arp2/3, a protein complex that promotes actin branching (Higgs and Pollard, 1999). Treatment of Jurkat cells with the CDC42-specific inhibitor secramine A blocks TNT formation (Arkwright et al., 2010). Similarly, inhibition of CDC42 in HeLa cells results in the decreased formation of TNTs induced by the overexpression of M-Sec, whereas Rac1 inhibition shows no effect (Hase et al., 2009). On the other hand, in macrophages, both the CDC42 and Rac1 pathways are involved in TNT formation through WASP-dependent actin remodeling (Hanna et al., 2017). In

¹Unit of Membrane Trafficking and Pathogenesis, Department of Cell Biology and Infection, Pasteur Institute, Paris 75015, France. ²Department of Integrative Life Sciences, Graduate School of Life Sciences, Tohoku University, Aoba-ku, Sendai, Miyagi 980-8578, Japan.

*These authors contributed equally to this work

‡Author for correspondence (chiara.zurzolo@pasteur.fr)

© S.Z., 0000-0002-7029-7204; C.Z., 0000-0001-6048-6602

neurons, the actin regulator proteins CDC42, insulin receptor substrate of 53kDa (IRS β 53) and vasodilator-stimulated phosphoprotein (VASP) work as a network to increase filopodia formation (Disanza et al., 2013). Interestingly, we showed that the same network inhibits TNT formation in neuronal cells while increasing filopodia formation. These and other data suggest that the same actin modifiers might have opposite actions on filopodia and TNT formation, indicating that these two structures, although similar, are distinct organelles with different functions (Delage et al., 2016; Gousset et al., 2013).

In addition to actin polymerization, formation of cellular protrusions (TNT, filopodia, cilia, etc.) also requires vesicular traffic. Rab GTPases are considered to be master regulators of intracellular membrane trafficking (Fukuda, 2008; Stenmark, 2009). Rab GTPases are localized in different membrane compartments to control the specificity and directionality of membrane trafficking pathways, mostly related to the trafficking of vesicles. Of particular interest, Rab GTPases are also involved in the regulation of cytoskeleton dynamics, including the formation of cell protrusions (Diekmann et al., 2011; Klöpper et al., 2012; Villarroel-Campos et al., 2016). Rab8 localizes to the primary cilium membrane during ciliogenesis, and cilia formation is inhibited or promoted when a Rab8 dominant-negative or positive form is expressed, respectively (Follit et al., 2010; Nachury et al., 2007). This suggests that the activity of Rab8 is crucial for the biogenesis of cilia. Rab8 is functionally linked to ADP-ribosylation factor 6 (Arf6). When the active form of Arf6 is present, cell protrusions induced by Rab8 can be inhibited (Hattula et al., 2006), indicating that inhibition may be related to membrane trafficking via endosome recycling rather than through the trans-Golgi network (TGN) (Hattula et al., 2006; Villarroel-Campos et al., 2016). On the other hand, Rab11 has been shown to promote neuritogenesis, both in hippocampal neurons in culture and in PC12 cells differentiated with nerve growth factor (NGF) through its interaction with protrudin (Shirane and Nakayama, 2006). Rab11 also increases axon outgrowth, a process that requires remodeling of the actin cytoskeleton. In hippocampal neurons, depletion of Rab11 reduces axonal length, which is also controlled by cyclin-dependent protein kinase5 (Cdk5) via an inhibitory phosphorylation of lemur kinase 1 (LMTK1), which in turn can activate Rab11 (Takano et al., 2012).

We decided to investigate the role of Rab GTPases in TNT formation and therefore performed a screen by overexpressing 41 GFP–Rab GTPases in our neuronal model CAD cells, (Matsui and Fukuda, 2011; Tsuboi and Fukuda, 2006). Based on this screening, Rab8a and Rab11a seemed promising candidates so we chose to investigate their specific involvement in TNT formation. Although two recent independent observations indicated that Rab8a and/or Rab11a are involved in TNT formation, the specific mechanism was not investigated (Burtey et al., 2015; Zhu et al., 2016). Our results showed that Rab8a and Rab11a positively regulate TNT formation and function in vesicle transfer between connected cells, via their active GTP-bound form. We demonstrated that Rab11a and Rab8a act through a cascade pathway to regulate downstream v-SNARE VAMP3-mediated fusion, suggesting that they increase vesicle recycling to the cell surface in order to form TNTs. Importantly, we demonstrated that this Rab cascade also regulates filopodia formation in our cell model, but through different effectors. Thus, in addition to improving our knowledge about TNT formation, our data demonstrate that TNTs are specific novel structures that are different from filopodia and other cellular protrusions.

RESULTS

High-content screening reveals that Rab8a and Rab11a promote DiD-labeled vesicle transfer between cells

To determine whether and which Rab GTPases affect TNT formation, we set up a screen whereby 41 GFP–Rab GTPases were overexpressed in our CAD cell line model. The transfer of cargos between cells, which is the main function of TNTs, was used to perform a preliminary screen and subsequently to study the formation of TNTs. To perform the transfer experiments, donor cells were transfected with 41 different GFP–Rab GTPases and incubated with the nonspecific membrane dye DiD (Vybrant™ DiD), which is quickly internalized and labels all internal vesicular compartments. Acceptor cells were transfected with H2B–mCherry and co-cultured with donor cells in a 1:1 ratio (Fig. 1A) (Delage et al., 2016). After 16 h of co-culture in 96-well plates, cells were fixed and images acquired to analyze the percentage of acceptor cells containing DiD-labeled vesicles transferred from donor cells (Fig. 1A). Images were analyzed with Cellprofiler (Fig. 1B). The percentage of acceptor cells containing DiD-labeled vesicles from each condition was normalized to control condition (cells transfected with an empty vector tagged with GFP) (Table S1). GFP–myosin10 and GFP–VASP were employed as positive and negative controls, as they respectively increase and decrease TNT formation and vesicle transfer (Delage et al., 2016; Gousset et al., 2013). We used three additional conditions as controls for cell-to-cell contact-mediated transfer: (i) mixture, where cells were just mixed and not incubated in co-culture, which gives the background noise; (ii) filter, where cells in co-culture were separated by a Transwell filter that impairs cell-to-cell contact; and (iii) supernatant, where the supernatant of donor cells was challenged with acceptor cells cultured separately, which measures transfer through secretion (Fig. 1C–F). To call hits from 41 GFP–Rab GTPases, two threshold values (105% and 95%) were set to score all conditions. When the relative percentage was higher than 105%, a hit was scored as ‘1’; when a hit was lower than 95%, it was scored as ‘–1’; and when a hit was between 95% and 105%, it was scored as ‘0’ (Table S1). The score values obtained from the average of triplicates from four experiments were summed, and a comparative analysis of the 41 GFP–Rab GTPases tested was performed. Among others, cells overexpressing Rab8a and Rab11a increased vesicle transfer between cells. These results were intriguing, because both these Rabs are involved in formation of cilia and other cell protrusions (Cox et al., 2000; Eva et al., 2010; Hattula et al., 2006; Peränen, 2011). Furthermore, two independent reports suggest that Rab8 or both Rab8 and Rab11 might be involved in regulating TNT formation, although the mechanism was not explored (Burtey et al., 2015; Zhu et al., 2016).

Rab11a positively regulates TNT formation and function via the active GTP-bound form

Rab11 localizes at the endocytic recycling compartment/recycling endosome (ERC/RE), the TGN and post-Golgi vesicles. It influences several cellular processes, including exocytic and recycling processes (controlling both secretion and composition of plasma membrane), cytokinesis, phagocytosis, cell migration, immunological synapse and primary cilia formation (Campa and Hirsch, 2017). To understand whether the increase in vesicle transfer is related to an increase in TNTs, we investigated the effect of Rab11a on TNTs by calculating the percentage of TNT-connected cells. Because no specific marker of TNTs is currently available, we quantified TNTs between cells (labeled with wheat germ agglutinin; WGA) (Delage et al., 2016). TNTs were identified in culture according to the current definition of TNTs as

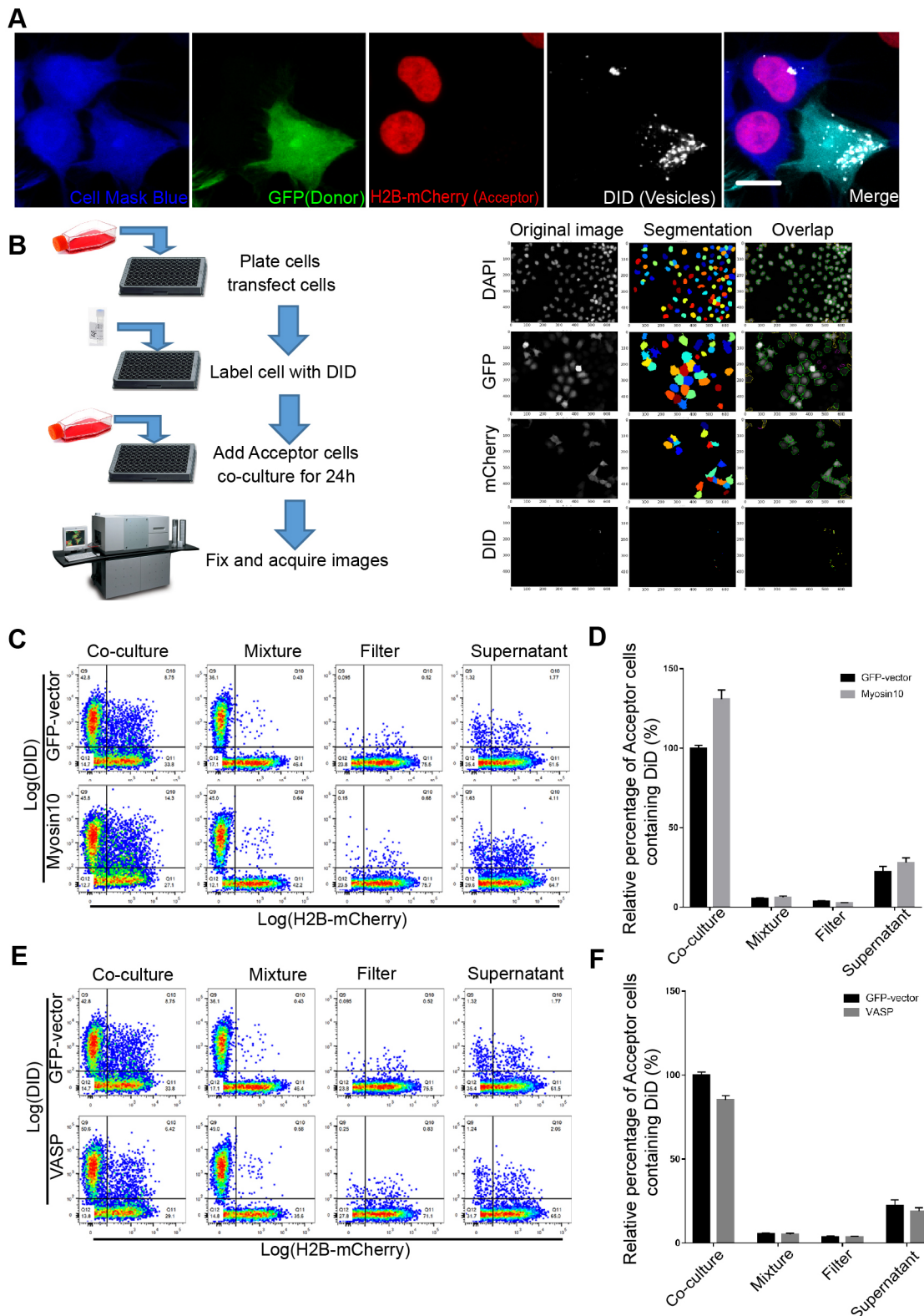


Fig. 1. See next page for legend.

membranous stretches between cells that do not contact the substrate (Fig. S1A) (Rustom et al., 2004). To rule out possible effects resulting from the distance between cells on TNT formation, we seeded different concentrations of cells (Fig. S1B) and determined the range of cell concentrations (Fig. S1C,D) for which the number

of TNT-connected cells was not affected (Fig. S1E). This measured the tolerance of the system and assured the reproducibility of our data. For all subsequent experiments, cells were plated at the same concentration within the determined tolerance regime. By using this method, we overexpressed wild-type (WT) GFP-Rab11a and

Fig. 1. Co-culture system for intercellular transfer of DiD-labeled vesicles and high-content screening assay. (A) An example of the co-culture system setup. Donor cells were transfected with GFP–vector or GFP–Rab plasmids and labeled with DiD; acceptor cells were transfected with H2B–mCherry. Cells were fixed after co-culture and labeled with HCS CellMask™. DiD-labeled vesicles transferred to acceptor cells were detected as white spots in cells with red nuclei. (B) Left panel shows high-content screening setup and workflow. Cells were co-cultured as described in A and fixed after co-culture. Right panel shows a representative image of process of segmentation of cells and vesicles. (C) Representative flow cytometry raw data (dot plots) of the co-culture of donor cells expressing GFP–vector or GFP–myosin10 and labeled with DiD and acceptor cells expressing H2B–mCherry. Acceptor cells containing DiD-labeled vesicles from the entire population of acceptor cells after co-culture were quantified. The various conditions were donor and acceptor cells co-cultured, cultured separately and mixed just before sorting (mixture); cultured separated by a filter (filter); and acceptor cells challenged with donor cells supernatant (supernatant). (D) Bar graphs showing the relative percentage of acceptor cells from the experiment described in C (GFP–vector=100±1.8, GFP–myosin10=130.9±5.6). (E,F) As C,D, except that GFP–vector or GFP–VASP was expressed in donor cells (GFP–vector=100.0±1.8, GFP–VASP=85.2±2.4). Data show mean±s.e.m. from three independent experiments. Scale bar: 10 µm.

observed a significant increase in the percentage of TNT-connected cells (Fig. 2A,B and Table S2).

To confirm that the intercellular connections induced by Rab11a were functional TNTs, we performed transfer assays measuring the transfer of labeled vesicles between cells in co-culture (Abounit et al., 2015). Two populations of cells, donor cells (transfected with GFP–Rab11a-WT) with internal vesicles labeled with a fluorescent membrane dye (Vybrant™ DiD) and acceptor cells (transfected with H2B–mCherry) were mixed at a 1:1 ratio and co-cultured for 16 h (Delage et al., 2016). Overexpression of GFP–Rab11a-WT significantly increased the transfer of DiD-labeled vesicles, as measured by two different methods, quantitative fluorescent image analysis (Fig. 2C) and flow cytometry (Fig. S2A). Again, we used two controls to exclude the effect of vesicle transfer by secretion: (1) cells were co-cultured using a Transwell filter to separate the two populations, and/or (2) the conditioned medium from donor cells (cultured in a separate dish) was applied to acceptor cells. In both conditions, transfer of vesicles was very low and not affected by the overexpression of GFP–Rab11a-WT, showing that vesicle transfer between cells relied on cell-to-cell contact, and not on secretion (Fig. S2A). We also found that Rab11a-WT protein was present in acceptor cells, which indicates that Rab11a-positive vesicles could transfer between cells through TNTs (Fig. S2B). These combined results show that the increase in TNTs induced by Rab11a corresponds to an increase in cargo transfer between cells, suggesting that the TNTs induced by Rab11a are functional.

Rab GTPases switch between two conformations, an inactive form bound to guanosine diphosphate (GDP) and an active form bound to guanosine triphosphate (GTP), to regulate different cellular processes. Thus, cells were transfected with GFP–Rab11a-Q70L (constitutively active mutant) and GFP–Rab11a-S25N (dominant-negative mutant) for 40 h. For GFP–Rab11a-Q70L, the increase in the percentage of TNT-connected cells was similar to that observed with GFP–Rab11a-WT (Fig. 2A,B and Table S2). Similarly, we observed an increase in vesicle transfer between cells (Fig. 2C). By contrast, GFP–Rab11a-S25N overexpression showed no increase in the number of TNT-connected cells (Fig. 2A,B and Table S2) nor an increase in vesicle transfer (Fig. 2C). Importantly, when the expression time of GFP–Rab11a-S25N was extended to 52 h, the percentage of TNT-connected cells was significantly decreased (Fig. S3A), indicating that the effectiveness of the

dominant-negative proteins depends on the time elapsed after transfection. We speculate that the levels of expression of dominant-negative Rabs at 40 h after transfection are insufficient to show dominant-negative effects (e.g. trapping their activator's GEFs) (Ramalho et al., 2002).

To further confirm the effect of Rab11a on TNTs, Rab11a was knocked down in an acute manner (more than 90%) using short hairpin RNA (shRNA; Fig. 2D). In this condition, both the number of TNT-connected cells (Fig. 2E,F and Table S2) and vesicle transfer between the two cell populations (Fig. 2G) were substantially decreased. Rescue experiments in which GFP–Rab11a-WT was overexpressed in Rab11a knockdown cells showed that both the number of TNT-connected cells (Fig. 2E,F and Table S2) and vesicle transfer were rescued (Fig. 2G). Together, these results suggest that Rab11a plays a role in the formation of functionally active TNTs and that the active GTP-bound form of Rab11a is needed.

Rab8a positively regulates TNT formation and function via the active GTP-bound form

Rab8 localizes in the TGN, where it recycles endosomes, vesicular and tubular structures in the cytosol, membrane protrusions and the plasma membrane. Rab8 is reported to be involved in several transport pathways, and it induces actin polymerization and cell surface protrusion formation (Hattula et al., 2002, 2006). We overexpressed GFP–Rab8a-WT, GFP–Rab8a-Q67L (constitutively active mutant) and GFP–Rab8a-T22N (dominant-negative mutant) for 40 h by transient transfection and found that GFP–Rab8a-WT and GFP–Rab8a-Q67L significantly increased the number of TNT-connected cells (Fig. 3A,B and Table S2). On the other hand, expression of GFP–Rab8a-T22N had no significant effect on TNT-connected cells (Fig. 3A,B and Table S2) unless its expression time was extended to 52 h. In the latter case, the percentage of TNT-connected cells was significantly decreased (Fig. S3A).

Consistent with a positive role of Rab8a in TNT formation, the transfer of vesicles increased in cells overexpressing GFP–Rab8a-WT and GFP–Rab8a-Q67L (Fig. 3C and Fig. S2C). On the other hand, expression of GFP–Rab8a-T22N resulted in a decrease in vesicle transfer between cells (Fig. 3C). By comparison with Transwell plate co-culture or conditioned medium, the effect of secretion on vesicle transfer in this condition was negligible, indicating that the transfer of vesicles between cells was mediated through cell–cell contact and not secretion (Fig. S2C). Similar to Rab11a, Rab8a protein could also transfer between cells through cell–cell contact and not secretion (Fig. S2D).

To further confirm the effect of Rab8a on TNTs, we acutely depleted Rab8a (more than 90%) with a specific shRNA (Fig. 3D). Downregulating the expression of Rab8a decreased the number of TNT-connected cells (Fig. 3E,F and Table S2) as well as DiD-labeled vesicle transfer between cells (Fig. 3G). Of importance, when overexpressing GFP–Rab8a-WT in Rab8a knockdown cells, both the number of TNT-connected cells (Fig. 3E,F and Table S2) and vesicles transferred (Fig. 3G) were rescued to control levels. All these results suggest that Rab8a is a positive regulator of TNTs through its GTP-active form.

An isoform of Rab8a (Rab8b) has been shown to have an effect on apical transport (Sato et al., 2014). Thus, we also checked the role of Rab8b in TNT formation. We found that overexpression of GFP–Rab8b-WT in CAD cells had no effect on either the number of TNT-connected cells (Fig. S3B) or the number of acceptor cells containing vesicles following co-culture (Fig. S3C). Overall, the

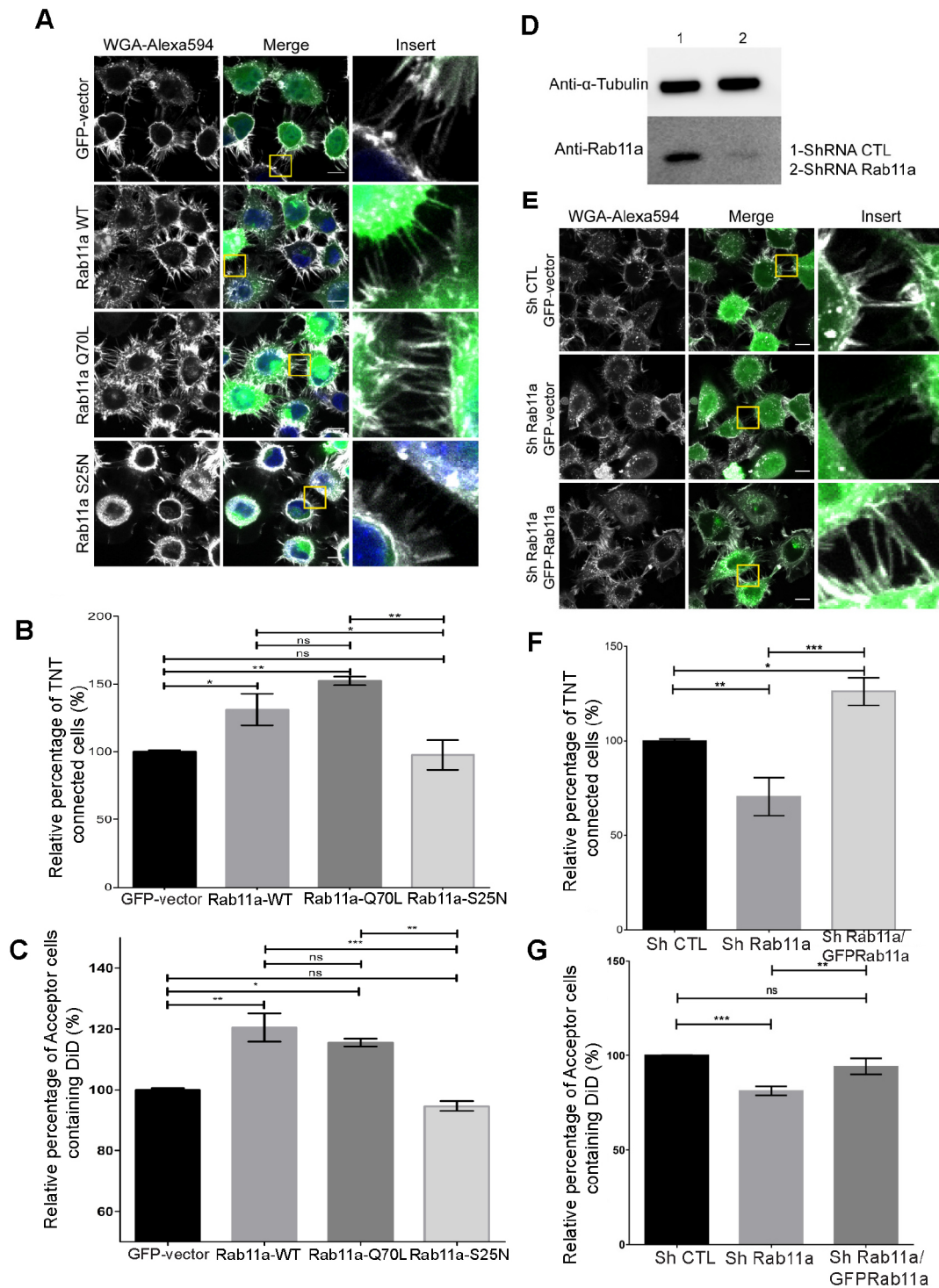


Fig. 2. See next page for legend.

data indicate that only the Rab8-specific isoform Rab8a has a positive effect on TNT formation.

Rab11a–Rab8a cascade in TNT formation

Of interest, Rab11 and Rab8 have been shown to work in a cascade pathway in several cellular processes, such as cyst lumen formation in MDCK cells (Roland et al., 2011), primary cilium generation (Westlake et al., 2011) and axon outgrowth (Furusawa et al., 2017). To assess whether Rab8a and Rab11a GTPases work in the same

pathway to modulate TNTs, we depleted one of the two Rabs and overexpressed the other one and quantified the number of TNT-connected cells and vesicle transfer between cells. We found that overexpressing Rab8a in shRNA-depleted Rab11a cells still led to an increase in the number of TNT-connected cells (Fig. 4A,B and Table S2) and rescued vesicle transfer between cells to control levels (Fig. 4C). By contrast, in cells depleted of Rab8a using shRNA, Rab11a overexpression had no effect on the number of TNT-connected cells (Fig. 4D,E and Table S2) or the number of

Fig. 2. Rab11a positively regulates functional TNTs via the active GTP-bound form. (A) Representative confocal images of TNT-connected cells after transfection of GFP–vector, GFP–Rab11a-WT, GFP–Rab11a-Q70L and GFP–Rab11aS25N. Inserts are enlargements of boxed regions in the merge panel. (B) Bar graph showing the relative percentage of TNT-connected cells from experiment described in A (GFP–vector=100±0.5, GFP–Rab11aWT=131.0±4.7, GFP–Rab11a-Q70L=152.4±2.2, GFP–Rab11aS25N=97.6±11.0). (C) Bar graph showing the relative percentage of acceptor cells containing DiD-labeled vesicles from the co-cultures, where donor cells were transfected with GFP–vector, GFP–Rab11a-WT, GFP–Rab11a-Q70L or GFP–Rab11a-S25N and labeled with DiD (GFP–vector=100±0.0, GFP–Rab11aWT=120.4±4.6, GFP–Rab11aQ70L=115.5±1.2, GFP–Rab11aS25N=94.6±1.6). (D) Western blot analysis of cells transfected with shRNA non-targeting (ShCTL) or targeting Rab11a (ShRab11a), showing the expression of Rab11a and α -tubulin as loading control. (E) Representative confocal images of TNT-connected cells after transfection with ShCTL/GFP–vector, ShRab11a/GFP–vector or ShRab11a/GFP–Rab11a. Inserts are enlargements of framed regions in merge panel. (F) Bar graph representing relative percentage of TNT-connected cells from experiment described in E (ShCTL/GFP–vector=100±0.5, ShRab11a/GFP–vector=70.5±4.5, ShRab11a/GFP–Rab11a=126.1±5.1). (G) Bar graph showing the relative percentage of acceptor cells containing DiD-labeled vesicles from the co-cultures, where donor cells were transfected with ShCTL/GFP–vector, ShRab11a/GFP–vector or ShRab11a/GFP–Rab11a and labeled with DiD (ShCTL/GFP–vector=100±0.2, ShRab11a/GFP–vector=81.3±2.4, ShRab11a/GFP–Rab11a=94.2±4.2). All graphs show mean±s.e.m. from three independent experiments (ns, not significant; * P <0.05, ** P <0.01, *** P <0.001; by one-way ANOVA with Tukey's multiple comparison post test). Scale bars: 10 μ m.

vesicles transferred between cells (Fig. 4F). These experiments showed that the effect of Rab8a on TNTs could be independent of Rab11a activation, whereas the effect of Rab11a on TNTs was dependent on the presence of Rab8a, indicating that Rab8a acts downstream of Rab11a in the regulation of TNT formation. Interestingly, when co-transfected in CAD cells, GFP–Rab8a and strawberry-Rab11a appeared to locate on the end of TNTs. This suggests that the two proteins cooperate on the same endosome at the base of the TNT for its formation (Fig. S4A).

A similar Rab activation cascade has been implicated in the *de novo* generation of the primary cilium (Westlake et al., 2011). It was demonstrated that Rab11 regulates Rab8 function by activating Rabin8 (Westlake et al., 2011), which is a major guanine nucleotide exchange factor (GEF) for Rab8 and an essential component for cell protrusion formation, such as ciliogenesis and neurite outgrowth (Wang et al., 2015). However, overexpression of GFP–Rabin8 did not affect the number of TNT-connected cells compared with the GFP control (Fig. S5A,B) nor affect the transfer of DiD-labeled vesicles between cells (Fig. S5C,D). Similarly, knockdown of Rabin8 by shRNA (Fig. S5E) had no effect on either the number of TNT-connected cells (Fig. S5F) or the number of vesicles transferred (Fig. S5G,H). This suggests that Rabin8 is not involved in the Rab11a–Rab8a cascade leading to TNT increase.

It has been reported that MICAL-L1 binds to GTP-bound Rab8a and stabilizes it on tubular membranes (Sharma et al., 2009; Rahajeng et al., 2012). Rab35 is known to interact with MICAL-L1 and to regulate neurite outgrowth (Kobayashi et al., 2014). Additionally, Rab35 also activates MICAL1 (Fremont et al., 2017; Deng et al., 2016). Because Rab35 was one of the positive hits in the screening (Table S1), we overexpressed MICAL-L1 and MICAL1 and checked their effect on TNT formation (Fig. S4B) and vesicle transfer (Fig. S4C). However, no significant effect on either vesicle transfer or TNT formation was observed, thereby indicating that Rab8 and Rab11 act independently of MICAL1 and MICAL-L1 proteins.

GRAB regulates TNT formation independently of Rab8a

It has been reported that GRAB (a guanine nucleotide exchange factor for Rab8a) mediates the Rab11a–Rab8a cascade mechanism and facilitates axonal growth (Furusawa et al., 2017). Therefore, we tested the effect of GRAB on TNT formation. We overexpressed wild-type GRAB in CAD cells and found that there was an increase in the number of TNT-connected cells (Fig. 5A,B and Table S2) and in vesicle transfer between cells in co-culture (Fig. 5C,D). To validate whether GRAB acts through the same pathway as Rab11a and Rab8a, we knocked down Rab8a by shRNA and overexpressed wild-type GFP–GRAB. We could still see an increase in TNT formation between cells (Fig. 5E,F and Table S2) and also an increase in vesicle transfer (Fig. 5G,H). This is an indication that GRAB does not act upstream of Rab8a and that it might act through an independent pathway that does not involve Rab8a.

VAMP3 acts downstream of Rab8a in regulating TNT formation

Rab8 and Rab11 have been shown to be crucial in vesicle recycling from the plasma membrane (Chen et al., 1998; Zhang et al., 2005). Blocking of either Rab8 or Rab11 pathways leads to an inhibition of the TGN-to-plasma membrane transport of recycling endosomes, as well as inhibition of plasma membrane recycling (Rowe et al., 2008); thus, one possibility is that TNT formation could be affected by this process. Primaquine (PMQ) interferes with membrane recycling from endosomes to the plasma membrane through direct interaction with endosomes (van Weert et al., 2000). We used this drug to inhibit transferrin recycling to the plasma membrane (Fig. 6A) and quantified the number of TNT-connected cells after 4 h of PMQ treatment. The results showed a significant decrease in the number of TNT-connected cells (Fig. 6B,C and Table S2), suggesting that vesicle recycling to the plasma membrane is involved in TNT formation.

The cascade of Rab11 activation couples cargo transport from the TGN and recycling endosomes to vesicle docking and fusion at the plasma membrane. By interacting with the v-SNARE VAMP3, Rab8 is responsible for the final docking/fusion step in T cell receptor recycling to the immune synapse (Finetti et al., 2015). Rab8 also interacts with VAMP3 at the base of the cilium, where VAMP3 regulates ciliary growth and targeting of Smoothed to the plasma membrane (Patrussi and Baldari, 2016). To test whether the Rab cascade affects TNTs through an increase in vesicle recycling, as mediated by VAMP3, we overexpressed GFP–VAMP3 and quantified the number of TNT-connected cells and vesicle transfer between cells. We found that there was an increase in both the percentage of TNT-connected cells (Fig. 6D,E and Table S2) and the number of DiD-labeled vesicles transferred (Fig. 6F and Fig. S6A). Comparison between the total transfer of vesicles and the supernatant-dependent transfer showed that the transfer of vesicles was mainly mediated by cell-to-cell contact (Fig. S6A). Interestingly, we also found that VAMP3-positive vesicles could transfer between cells in a cell–cell contact-dependent manner (Fig. S6B).

To confirm the function of VAMP3 in regulating TNT formation, knockdown of VAMP3 by shRNA (Fig. 6G) decreased the number of TNT-connected cells (Fig. 6H,I and Table S2) and decreased the transfer of vesicles between cells (Fig. 6J). On the other hand, overexpressing VAMP3 in VAMP3 knockdown cells restored both the number of TNT-connected cells (Fig. 6H,I and Table S2) and vesicle transfer between cells (Fig. 6J). These results suggest that VAMP3 is involved in the regulation of TNT formation.

To confirm whether VAMP3 is a downstream effector of Rab8a in regulating TNT formation, GFP–Rab8a-WT was overexpressed

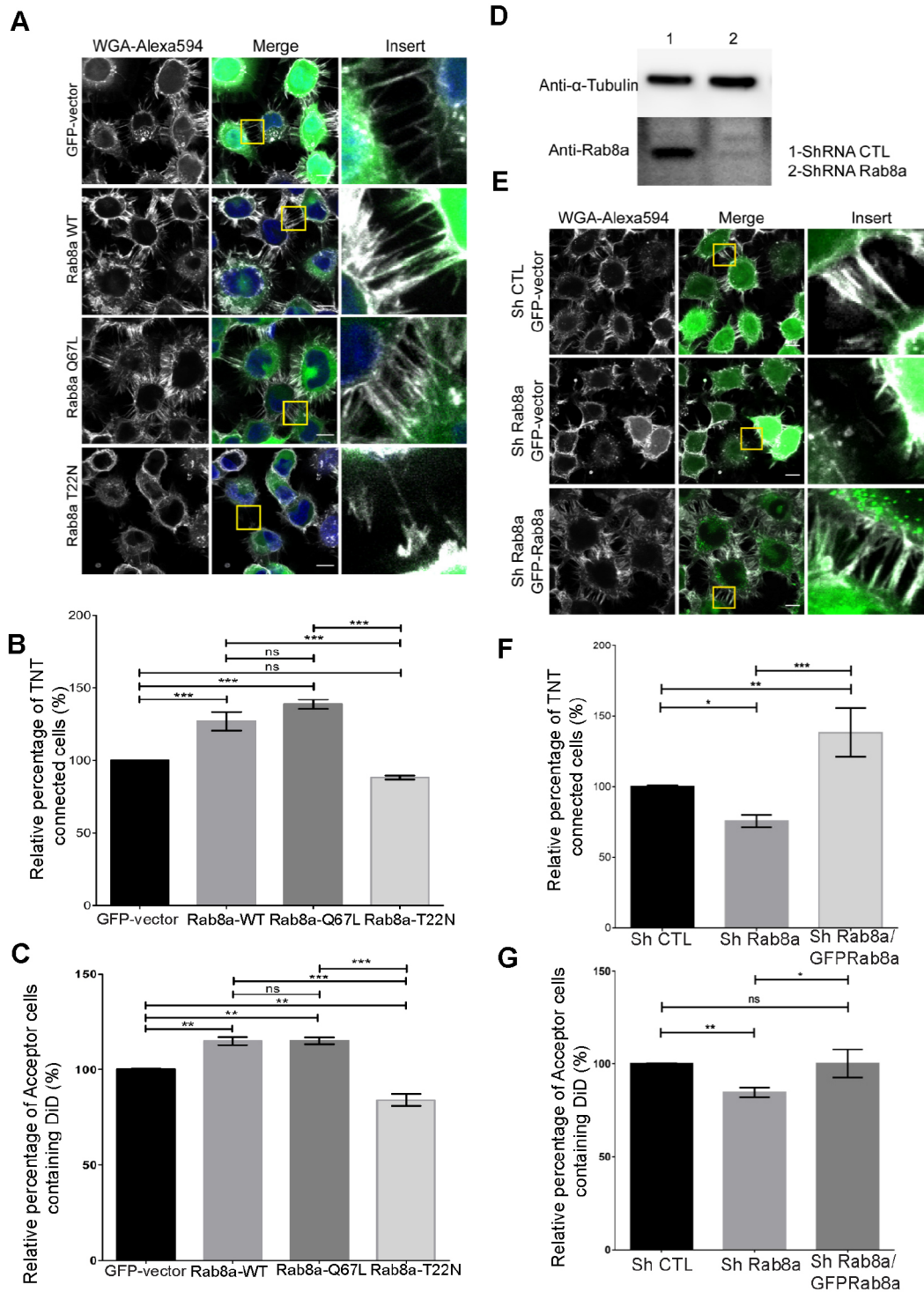


Fig. 3. Rab8a positively regulates functional TNTs via the active GTP-bound form. (A) Representative confocal images of TNT-connected cells after transfection with GFP-vector, GFP-Rab8a-WT, GFP-Rab8a-Q67L or GFP-Rab8a-T22N. Inserts are enlargements of boxed regions in merge panel. (B) Bar graph representing relative percentage of TNT-connected cells from experiment described in A (GFP-vector=100, GFP-Rab8a-WT=124.2±3.1, GFP-Rab8a-Q67L=138.8±2.1, GFP-Rab8a-T22N=88.3±0.9). (C) Bar graph showing the relative percentage of acceptor cells containing DiD-labeled vesicles from the co-cultures, where donor cells were transfected with GFP-vector, GFP-Rab8a-WT, GFP-Rab8a-Q67L or GFP-Rab8a-T22N and labeled with DiD (GFP-vector=100.0±0.57, GFP-Rab8a-WT=114.9±2.004, GFP-Rab8a-Q67L=115±1.729, GFP-Rab8a-T22N=84.02±3.145). (D) Western blot of cells transfected with shRNA non-targeting (ShCTL) or targeting Rab8a (ShRab8a) and α -tubulin as loading control. (E) Representative confocal images of TNT-connected cells after transfection with ShCTL/GFP-vector, ShRab8a/GFP-vector, and ShRab8a/GFP-Rab8a. Inserts are enlargements of the framed region in merge panel. (F) Bar graph representing the relative percentage of TNT-connected cells from experiment described in E (ShCTL/GFP-vector=100 ±0.57, ShRab8a/GFP-vector=75.67±1.8, ShRab8a/GFP-Rab8a=138.3±17.3). (G) Bar graph showing the relative percentage of acceptor cells containing DiD-labeled vesicles from the co-cultures, where donor cells were transfected with ShCTL/GFP-vector, ShRab8a/GFP-vector or ShRab8a/GFP-Rab8a and labeled with DiD (ShCTL/GFP-vector=100±0.2, ShRab8a/GFP-vector=84.5±2.4, ShRab8a/GFP-Rab8a=100.1±7.5). All graphs show mean±s.e.m. from three independent experiments (ns, not significant; * P <0.05, ** P <0.01, *** P <0.001; by one-way ANOVA with Tukey's multiple comparison post test). Scale bars: 10 μ m.

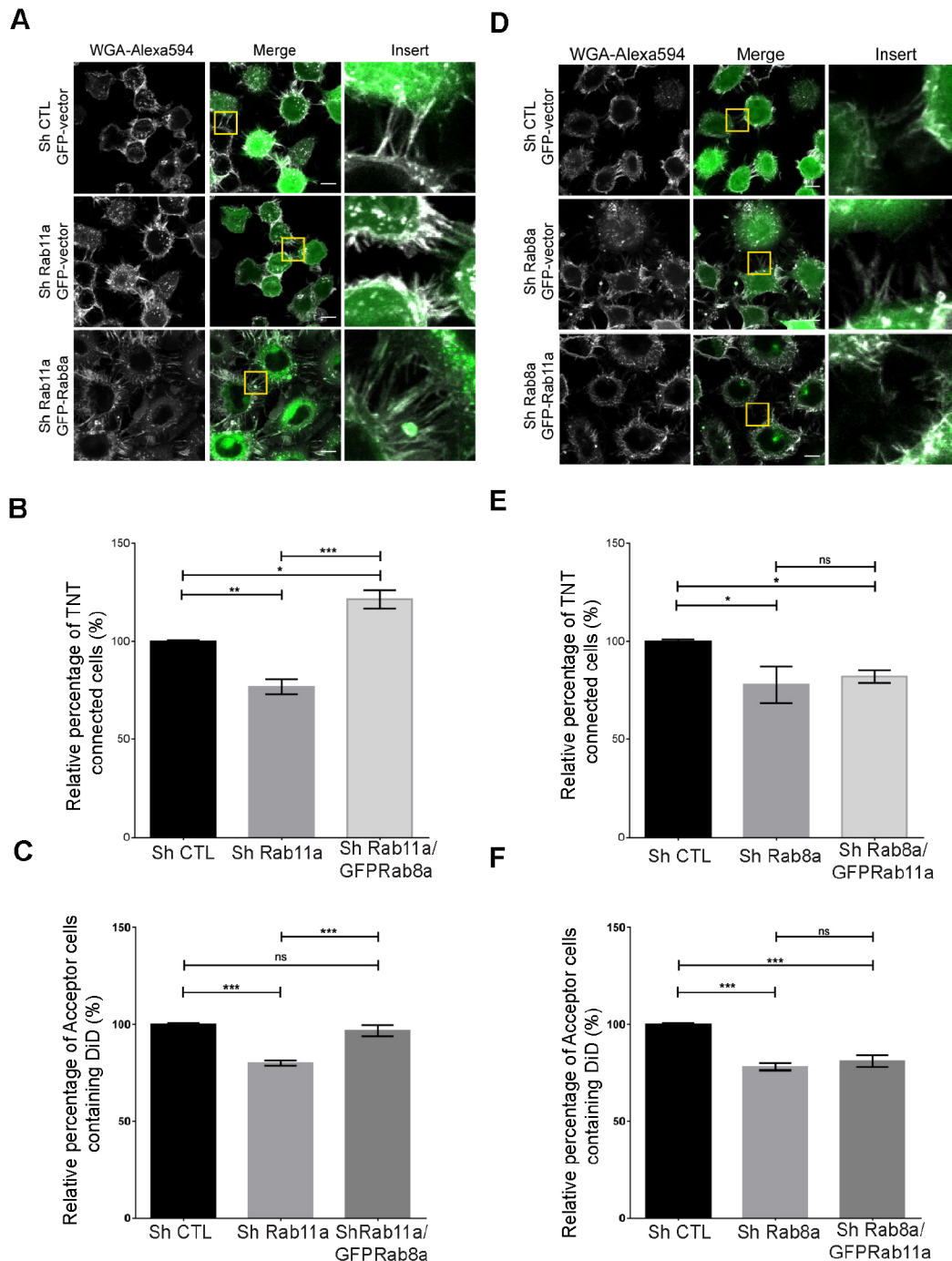


Fig. 4. Rab11a–Rab8a cascade in TNT formation. (A) Representative confocal images of TNT-connected cells after transfection with ShCTL/GFP–vector, ShRab11a/GFP–vector or ShRab11a/GFP–Rab8a. Inserts are enlargements of framed regions in merge panel. (B) Bar graph showing relative percentage of TNT-connected cells from experiment described in A (ShCTL/GFP–vector=100±0.57, ShRab11a/GFP–vector=76.74±3.9, ShRab11a/GFP–Rab8a=121.7±4.74). (C) Bar graph showing the relative percentage of acceptor cells containing DiD-labeled vesicles from the co-cultures, where donor cells were transfected with ShCTL/GFP–vector, ShRab11a/GFP–vector or ShRab11a/GFP–Rab8a and labeled with DiD (ShCTL/GFP–vector=100±0.69, ShRab11a/GFP–vector=79.91±1.3, ShRab11a/GFP–Rab8a=96.7±2.94). (D) Representative confocal images of TNT-connected cells after transfection with ShCTL/GFP–vector, ShRab8a/GFP–vector or ShRab8a/GFP–Rab11a. Inserts are enlargements of the framed regions in merge panel. (E) Bar graph showing the relative percentage of TNT-connected cells from the experiment described in D (ShCTL/GFP–vector=100±0.57, ShRab8a/GFP–vector=77.97±5.51, ShRab8a/GFP–Rab11a=81.95±3.15). (F) Bar graph representing the relative percentage of acceptor cells containing DiD-labeled vesicles from the co-cultures, where donor cells were transfected with ShCTL/GFP–vector, ShRab8a/GFP–vector or ShRab8a/GFP–Rab11a and labeled with DiD (ShCTL/GFP–vector=100±0.6, ShRab8a/GFP–vector=78.05±1.9, ShRab8a/GFP–Rab11a=80.91±2.9). All graphs are from three independent experiments and show mean±s.e.m. (ns, not significant; **P*<0.05, ***P*<0.01, ****P*<0.001; by one-way ANOVA with Tukey's multiple comparison post test). Scale bars: 10 μm.

in VAMP3 knockdown cells. Under these conditions, neither the number of TNT-connected cells (Fig. 7A,B and Table S2) nor the vesicles transferred between cells (Fig. 7C) were affected.

Furthermore, overexpressing GFP–Rab11a-WT in VAMP3 knockdown cells had no effect on the number of TNT-connected cells (Fig. 7A,B and Table S2) nor vesicle transfer between cells

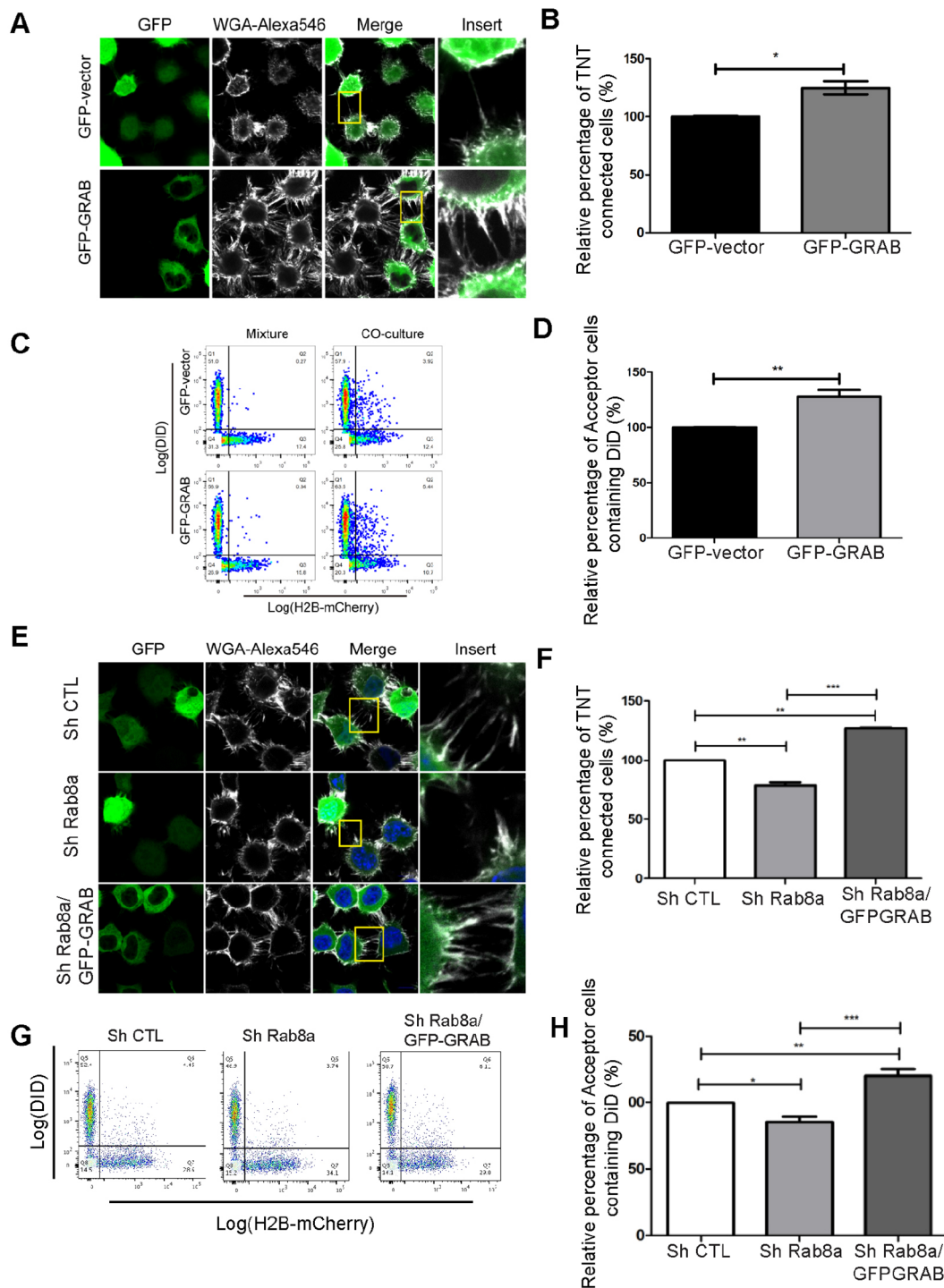


Fig. 5. GRAB regulates formation of TNT independent of Rab8a. (A) Representative confocal images of TNT-connected cells after transfection with GFP-vector or GFP-GRAB. Inserts are enlargements of the framed region in merge panel. (B) Bar graph representing relative percentage of TNT-connected cells from the experiment described in A (GFP-vector=100±0.5, GFP-GRAB=125±5.4). (C) Raw data (dot plots) of flow cytometry from a representative experiment showing the relative percentage of acceptor cells containing DiD-labeled vesicles from the co-cultures, where donor cells were transfected with either GFP-vector or GFP-GRAB and labeled with DiD. (D) Bar graph representing the relative percentage of acceptor cells containing DiD-labeled vesicles from the co-cultures of the experiment described in C (GFP-vector=100.0±0.5, GFP-GRAB=128.0±5.8). All graphs show mean±s.e.m. from three independent experiments (* P <0.05, ** P <0.01; by unpaired Student's t -test). (E) Representative confocal images of TNT-connected cells after transfection with ShCTL/GFP-vector, ShRab8a/GFP-vector or ShRab8a/GFP-GRAB. Inserts are enlargements of the framed regions in merge panel. (F) Bar graph showing relative percentage of TNT-connected cells from experiment described in E (ShCTL/GFP-vector=100, ShRab8a/GFP-vector=78.2±3.4, ShRab8a/GFP-GRAB=126.9±0.6). (G) Raw data (dot plots) of flow cytometry from a representative experiment showing the relative percentage of acceptor cells containing DiD-labeled vesicles from the co-cultures, in which the donor cells were transfected with ShCTL/GFP-vector, ShRab8a/GFP-vector or ShRab8a/GFP-GRAB and labeled with DiD. (H) Bar graph representing the relative percentage of acceptor cells containing DiD-labeled vesicles from the co-cultures of the experiment described in G (ShCTL/GFP-vector=99.5±0.5, ShRab8a/GFP-vector=85.1±10.2, ShRab8a/GFPGRAB=120.0±12.1). All graphs show mean±s.e.m. (* P <0.05, ** P <0.01, *** P <0.001; by one-way ANOVA with Tukey's multiple comparison post test) from two independent experiments. Scale bars: 10 μ m.

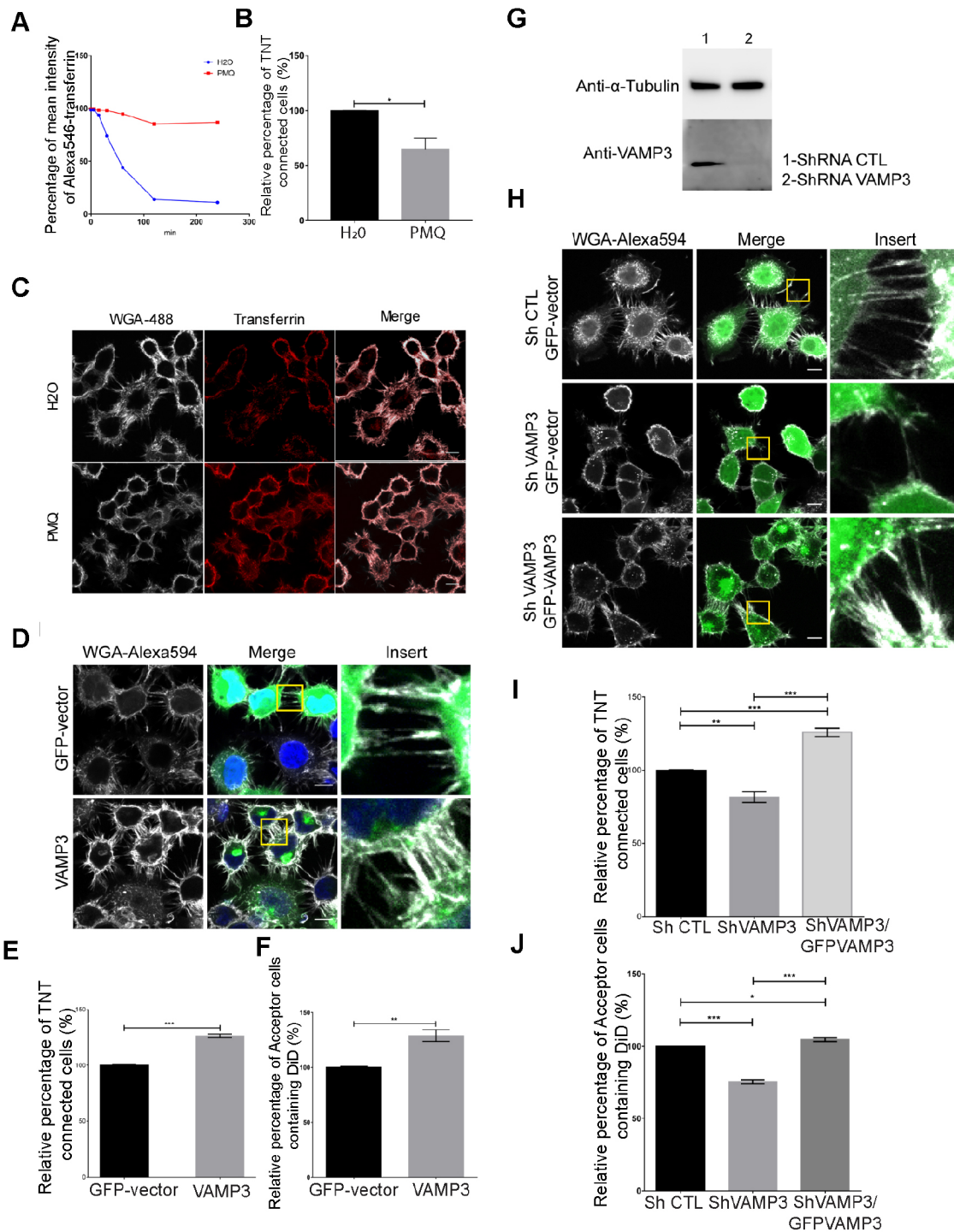


Fig. 6. See next page for legend.

(Fig. 7C). These results indicate that VAMP3 is involved in the Rab11a–Rab8a cascade, regulating TNT formation by acting downstream of Rab8a.

Rab8a and Rab11a promote both TNTs and filopodia formation, with different mechanisms

Both Rab11 and Rab8 have been shown to be involved in filopodia formation in different contexts (Cox et al., 2000; Eva et al., 2010; Hattula et al., 2006; Peränen, 2011). Although we have shown that

in CAD cells filopodia and TNTs are formed by different mechanisms leading to actin remodeling (Delage et al., 2016), the question arises whether, in our cell model, the same Rab cascade also leads to an increase in filopodia formation. In contrast to TNTs, attached filopodia exhibit vinculin-positive focal adhesions at the tip (Bohil et al., 2006; Schafer et al., 2010). By automatically detecting vinculin-positive peripheral cellular protrusions, we observed that overexpression of Rab8a or Rab11a also increased the number of vinculin-positive protrusions (Fig. S7A,B). Inversely,

Fig. 6. VAMP3 positively regulates functional TNTs. (A) Relative mean intensity of Alexa Fluor 546-transferrin bound to cells after treatment with Primaquine (PMQ) or H₂O for 0 min (H₂O=98.6, PMQ=99.2), 5 min (H₂O=98.6, PMQ=99.3), 15 min (H₂O=93.6, PMQ=98.4), 30 min (H₂O=74.1, PMQ=98.1), 60 min (H₂O=44.0, PMQ=94.6), 120 min (H₂O=13.8, PMQ=85.4) or 240 min (H₂O=11.0, PMQ=86.7) analyzed by flow cytometry. (B) Bar graphs showing relative percentage of TNT-connected cells after treatment with PMQ or H₂O for 4 h (H₂O=100±0.57, PMQ=64.92±10.07). The graph shows mean±s.e.m. from three independent experiments (**P*<0.05; by unpaired Student's *t*-test). (C) Representative confocal images of TNT-connected cells after treatment with PMQ or H₂O for 4 h. (D) Representative confocal images of TNT-connected cells after transfection with GFP–vector or GFP–VAMP3. Inserts are enlargements of the framed regions in merge panel. (E) Bar graph representing relative percentage of TNT-connected cells from experiment described in D (GFP–vector=100.0±0.5, GFP–VAMP3=126.4±1.7). (F) Bar graph representing the relative percentage of acceptor cells containing DiD-labeled vesicles from the co-cultures, where donor cells were transfected with either GFP–vector or GFP–VAMP3 and labeled with DiD (GFP–vector=100.2±0.73, GFP–VAMP3=129.0±5.3). The graphs show mean±s.e.m. from three independent experiments (***P*<0.01, ****P*<0.001; by unpaired Student's *t*-test). (G) Western blot of cells transfected with shRNA non-targeting (ShCTL) or targeting VAMP3 (ShVAMP3), showing the expression of VAMP3 and α -tubulin as loading control. (H) Representative confocal images of TNT-connected cells after transfection with ShCTL/GFP–vector, ShVAMP3/GFP–vector or ShVAMP3/GFP–VAMP3. Inserts are enlargements of the framed region in merge panel. (I) Bar graph representing relative percentage of TNT-connected cells from experiment described in H (ShCTL/GFP–vector=100±0.4, ShVAMP3/GFP–vector=81.6±3.6, ShVAMP3/GFP–VAMP3=126±2.9). (J) Bar graph representing the relative percentage of acceptor cells containing DiD-labeled vesicles from the co-cultures, where donor cells were transfected with ShCTL/GFP–vector, ShVAMP3/GFP–vector or ShVAMP3/GFP–VAMP3 and labeled with DiD (ShCTL/GFP–vector=100, ShVAMP3/GFP–vector=75.3±1.2, ShVAMP3/GFP–VAMP3=104.5±1.2). The above graphs show mean ±s.e.m. from three independent experiments (**P*<0.05, ***P*<0.01, ****P*<0.001; by one-way ANOVA with Tukey's multiple comparison post test). Scale bars: 10 μ m.

knocking down Rab8a or Rab11a was associated with a decrease in vinculin-positive protrusions (Fig. S7C,D). This result indicates that Rab8a and Rab11a increased both the number of TNTs and the number of attached filopodia. Interestingly, we found that overexpression of Rabin8 increased the number of vinculin-positive protrusions (Fig. S7E,F), whereas it had no effect on TNT formation and vesicle transfer between the cells (Fig. S5). Thus, Rabin8 could be the effector of Rab11a, and GEF of Rab8a, in promoting attached filopodia formation, but not for TNTs. On the other hand, overexpression of VAMP3, which increased TNTs (Fig. 6), decreased the number of attached filopodia (Fig. S7E,F). Together, these results suggest that VAMP3 could act as an effector of Rab8a in regulating TNT formation, but not the formation of attached filopodia.

DISCUSSION

The data presented here provide new insights into the factors involved in TNT formation and intercellular vesicle transfer in neuron-like CAD cells. Our results show that Rab11a, Rab8a and VAMP3 increase both the number of TNT-connected cells and vesicle transfer through TNTs in CAD cells. We have demonstrated that Rab11a and Rab8a work in the same pathway and employ VAMP3 as an effector to induce functional TNTs but not filopodia. Of interest, this Rab11a–Rab8a signaling cascade does not require Rabin8, which is essential in mediating Rab8a-activated filopodia formation. Thus, in addition to providing mechanistic details about the role of Rab proteins in TNT formation, the data also strengthen our hypothesis that filopodia and TNTs are different structures, which rely on different mechanisms of formation.

The fact that Rab effectors are highly diverse illustrates that Rab GTPases control multiple biochemical events. The functions of Rab GTPases and their effectors are mostly related to the vesicular traffic between donor and recipient compartments. Some distinct Rab effectors are involved in the sorting of cargo into vesicles by acting on budding, uncoating and motility along actin or microtubule filaments (Stenmark, 2009). Through their activation, Rab GTPases control the maturation of vesicles, as well as vesicle shuttling between different membrane compartments (Zhen and Stenmark, 2015). The function of activated Rab GTPases is to recruit effectors such as coat proteins (Carroll et al., 2001), cytoskeletal motors (Roland et al., 2007; Wu et al., 2002), kinases and phosphatases (Shin et al., 2005) and membrane tethering/fusion proteins (Nielsen et al., 2000; Simonsen et al., 1998). Because TNTs are novel cellular structures consisting of membranous channels containing actin that bridge distant cells and allow the exchange of different materials/cargos (Abounit and Zurzolo, 2012), it is likely that specific Rab proteins are involved in TNT formation. To assess this, we set up a screen where all 41 Rab subfamilies were tested for possible roles in TNT-mediated vesicle transfer in CAD cells. Although Rab8a, Rab11a and Rab35 could increase vesicle transfer between cells, we found that Rab39 and Rab40 had negative effects (Table S1).

We decided to focus on Rab8 and Rab11, for which there is evidence supporting their role in TNT formation in other cell systems, although the mechanism was unexplored (Burtey et al., 2015; Zhu et al., 2016). Rab11 and Rab8 could work independently from each other or in the same pathway (Hattula et al., 2006). In addition, because TNTs are membrane protrusions containing actin filaments, these two Rab GTPases could affect TNT formation by playing a role either in modulating actin dynamics and/or by regulating the supply of the membrane-specific lipids and proteins required for TNT development.

Both Rab8 and Rab11 can be found associated with the trans-Golgi network and recycling endosomes, and have been shown to be essential in the trafficking of proteins from the Golgi to the plasma membrane (Rowe et al., 2008). Intriguingly, Rab8 and Rab11 could also modulate actin dynamics (Castillo-Romero et al., 2010; Hattula et al., 2002; Ramel et al., 2013). Rab11 is known to be involved in the recycling of endocytosed proteins. However, Rab11 also regulates actin dynamics during formation of membrane protrusions and is required for the spatial control of Rac1 activity through the control of cell–cell communication during collective cell migration by inducing cell protrusions through the regulation of moesin activation (Ramel et al., 2013). On the other hand, Rab8 has been shown to drive cytoskeletal reorganization in HeLa cells, either through RhoA GTPase, calpain or MT1-MMP activation (Bravo-Cordero et al., 2016). However, knocking down RhoA GTPase in DNA damage-induced senescent cells did not induce a significant reduction in mCherry transfer between cells, suggesting that Rab8 could regulate TNT formation not only through actin polymerization (Biran et al., 2015).

Of interest, Rab8 has been reported to target vesicles to the cilium to promote ciliary membrane elongation (Nachury et al., 2007). Endogenous Rab8 localizes to the primary cilium and to the BBsome, which associates with the ciliary membrane. VAMP3, which is involved in the docking and/or fusion of synaptic vesicles with the plasma membrane, interacts with Rab8 at the base of the cilium to regulate ciliary growth and transport of specific receptors, such as Smoothed and fibrocystin to the cilium (Boehlke et al., 2010; Follit et al., 2010). By interacting with VAMP3, Rab8 is also responsible for the final docking/fusion step

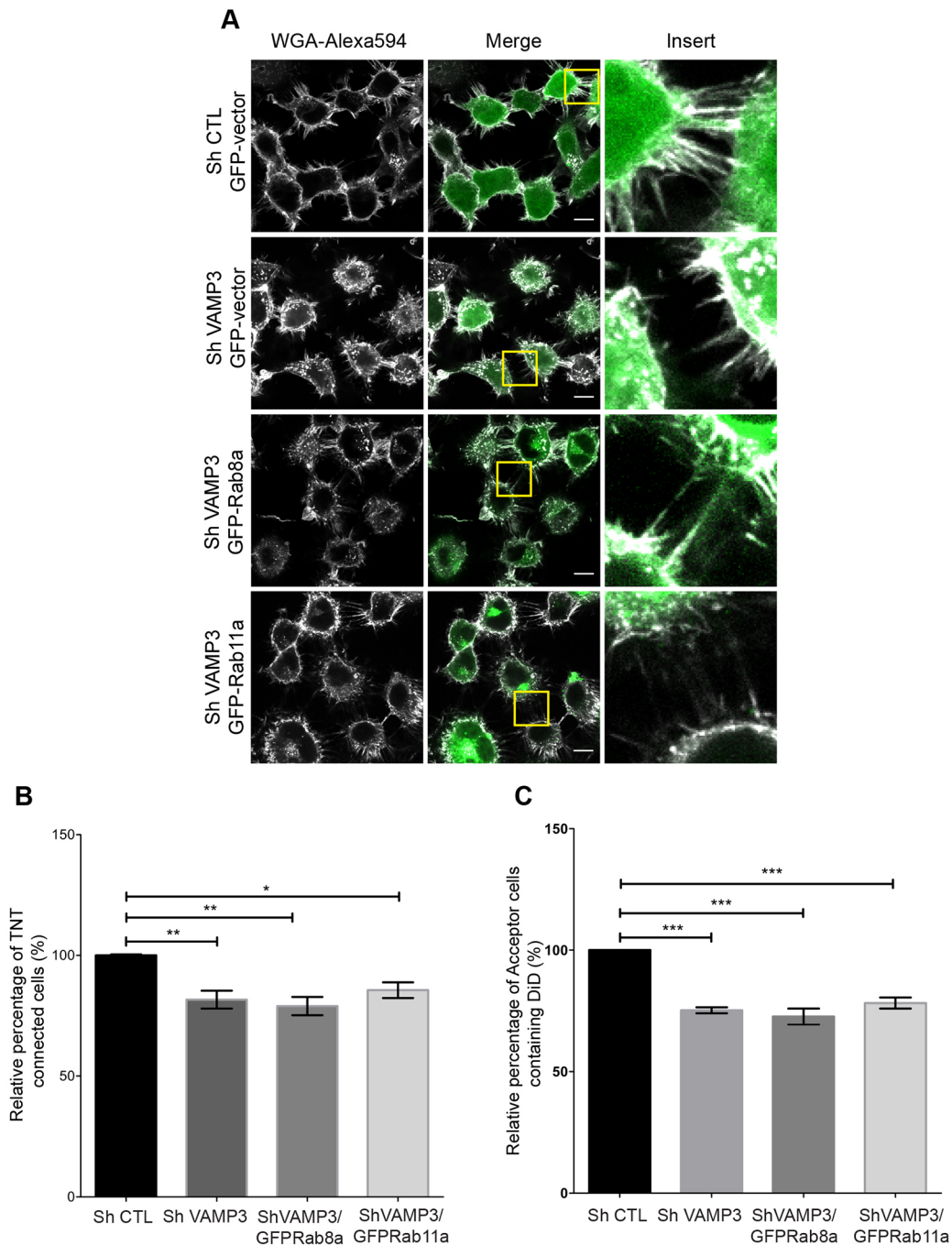


Fig. 7. VAMP3 acts downstream of Rab8a in regulating TNTs. (A) Representative confocal images of TNT-connected cells after transfection with ShCTL/GFP-vector, ShVAMP3/GFP-vector, ShVAMP3/GFP-Rab8a or ShVAMP3/GFP-Rab11a. Inserts are enlargements of the framed region in merge panel. (B) Bar graph showing relative percentage of TNT-connected cells from the experiment described in A (ShCTL/GFP-vector=100±0.4, ShVAMP3/GFP-vector=81.6±3.6, ShVAMP3/GFP-Rab8a=79.0±3.7, ShVAMP3/GFP-Rab11a=85.6±3.2). (C) Bar graph representing the relative percentage of acceptor cells containing DiD-labeled vesicles from the co-cultures, where donor cells were transfected with ShCTL/GFP-vector, ShVAMP3/GFP-vector, ShVAMP3/GFP-Rab8a or ShVAMP3/GFP-Rab11a and labeled with DiD (ShCTL/GFP-vector=100, ShVAMP3/GFP-vector=75.3±1.2, ShVAMP3/GFP-Rab8a=72.7±3.3, ShVAMP3/GFP-Rab11a=78.3±1.4). The graphs show mean±s.e.m. from three independent experiments (ns, not significant; * P <0.05, ** P <0.01, *** P <0.001; by one-way ANOVA with Tukey's multiple comparison post test). Scale bars: 10 μ m.

in T cell receptor recycling to the immune synapse (Patrussi and Baldari, 2016).

Our results clearly show that VAMP3 promotes TNT formation by acting downstream of Rab8a in CAD cells. It is therefore possible that Rab8a uses a similar mechanism to facilitate TNT formation by transporting vesicles and/or specific proteins or receptors to the

bases of TNTs. This could be initiated by the fusion of a contractile vacuole with the cell membrane to form negative and positive curvature at the TNT tip and base, respectively. Subsequently, the extension of TNTs could be supported by membrane intake through motor proteins and exocytosis involving myosin10 (Bishai et al., 2013; Gousset et al., 2013) and Rab8 (Wang et al., 2015). Our

results show an impairment of membrane recycling from endosomes to the plasma membrane with PMQ, leading to a decrease in the number of TNT-connected cells, which is in perfect accordance with this model.

There is evidence supporting a model in which, during membrane flow from one organelle to another, the compartment transition from an upstream Rab to a downstream Rab is regulated by the recruitment of effectors (Hutagalung and Novick, 2011). The Rab11–Rab8 cascade has been shown to be involved in several cellular processes, including transferrin receptor recycling, primary cilium formation and axon outgrowth. Regarding TNTs, our results show that Rab8a depletion inhibits TNT formation induced by Rab11a, whereas Rab11a depletion does not affect the formation of TNTs induced by Rab8a. This indicates that Rab8a acts as a downstream effector of Rab11a to regulate TNT formation. How this occurs is still unclear. However, when overexpressed together, Rab11a and Rab8a appear to colocalize at the base of the TNT, which suggests that the two proteins cooperate on the same endosome at the base of the TNT for its formation. On the other hand, from this qualitative analysis, the two proteins do not appear to colocalize inside TNTs.

Even though we have shown that the downregulation of Rab11a and Rab8a by shRNA is close to 90%, we did not see a similar decrease in 90% of the TNT-connected cells. This is expected, as other effectors have been described to increase TNT formation, such as M-sec (Hase et al., 2009) and myosin-10 (Gousset et al., 2013). On the other hand, the data suggest that these proteins might act in an independent (or parallel) pathway to the Rab11a–Rab8a cascade described here.

M-sec is known to be a component of the exocyst complex. It interacts with RalA (Ras-like small GTPase) to regulate the formation of TNTs (Kimura et al., 2016). RalA interacts with CDC42 through Ral1 binding protein for the formation of filopodia (Ikeda et al., 1998). Additionally, CDC42 has been shown to regulate the formation of TNTs in Raw264.7 cells (Hanna et al., 2017). However, in the case of CAD cells, CDC42 negatively regulates the formation of TNTs (Delage et al., 2016). Thus, we believe that this pathway is not responsible for TNT formation in our cell model.

However, some proteins of the exocyst complex (e.g. Sec15 and Exo70) have been shown to interact with Rab11 (Takahashi et al., 2012; Wu et al., 2005). From preliminary experiments, overexpression of Sec15 in CAD cells results in only a slight decrease in vesicle transfer between cells in co-culture; consequently, we did not pursue this further. However, Exo70 could be an interesting candidate because it is known to induce membrane curvature and actin-free filopodia (Zhao et al., 2013) and it also interacts with Rab11 in the exocytosis process (Takahashi et al., 2012). Further research is necessary to explore this possibility.

Guanine nucleotide exchange factor for Rab3A (GRAB), a GEF of Rab8, has been shown to regulate axon outgrowth (Furusawa et al., 2017). These results indicated that GRAB regulates axonal outgrowth via activation and recruitment of Rab8A to Rab11A-positive endosomes in a Cdk5-dependent manner. GRAB might act as a GEF for regulating the formation of TNTs and the transfer of vesicles. But, from our results, we conclude that GRAB acts on TNT formation irrespective of Rab8a and is not involved in a Rab8a–Rab11a pathway in regulating the formation of TNT. Because GFP–GRAB promoted vesicle transfer in Rab8a-KD cells, GRAB might activate unknown Rabs other than Rab8a to increase vesicle transfer. Rabin8, a close homolog of GRAB, can activate both Rab8 and Rab10 to promote neurite outgrowth of

PC12 cells. Overexpression of Rab10 (WT/QL) had no effect on neurite outgrowth, whereas its knockdown decreased neurite outgrowth (Homma and Fukuda, 2016). Thus, Rab10 is a likely candidate for an alternative GRAB target in regulating the formation of TNTs between the cells. However, since Rab10 did not come up as a possible positive regulator in our initial screening of 41 Rabs, we believe that further studies are needed to explore the mechanism of Rab10 and GRAB in regulating the formation of TNTs.

In other circumstances, for example in *de novo* generation of the primary cilium, Rab11 regulates Rab8 function by activating Rabin8, a GEF of Rab8 (Westlake et al., 2011). However, in our cell system, overexpression of Rabin8 did not affect TNT number, strongly suggesting that Rabin8 is not the effector between Rab8 and Rab11 in the regulatory pathway of TNTs. Furthermore, we showed that, in our cell system, the Rab11a–Rab8a cascade induces filopodia formation through Rabin8, whereas VAMP3 had no effect on filopodia. This indicates that filopodia and TNTs, although naively similar in appearance, are distinct structures with different mechanisms of formation and different functions. We propose that Rab11a and Rab8a facilitate the trafficking and fusion of vesicles, containing specific proteins and lipids necessary for TNT formation and function, with the plasma membrane (by interacting with the v-SNARE protein VAMP3). On the other hand, this cellular process could also regulate TNT formation simply by facilitating membrane accumulation at the site of TNT formation (see schematic in Fig. 8).

In summary, our results represent the first molecular evidence of a mechanism whereby Rab GTPases regulate TNT formation in neuron-like CAD cells. Our study further confirms that TNTs are regulated differently from other cell protrusions, including filopodia and primary cilia. Future studies are required to provide further

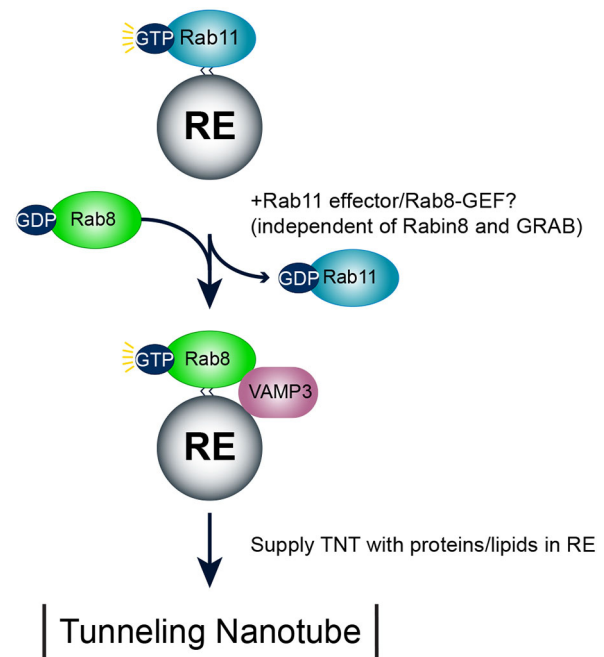


Fig. 8. Schematic of Rab11a–Rab8a–VAMP3 cascade in regulating TNTs. GTP-bound Rab11a acts upstream of Rab8a, while VAMP3 acts downstream of Rab8a in regulating TNT formation. Rab11a-induced activation of Rab8a is independent of Rabin8 and GRAB. One possibility is that Rab11a is released from the recycling endosome (RE) when Rab8a is activated. GTP-bound Rab8a interacts with VAMP3, which functions as a Rab8a effector and facilitates the fusion of RE-derived vesicle to supply lipids and specific proteins needed for TNT formation.

insights into the involvement of these and other Rab proteins (as from our screen) in vesicular trafficking and actin remodeling in TNT formation to better characterize the differences and similarities between TNT and other membrane protrusions.

MATERIALS AND METHODS

Cell lines, plasmids and transfection procedures

The mouse catecholaminergic neuronal CAD cell line (mouse catecholaminergic neuronal cell line, Cath.aDifferentiated) (Gousset et al., 2013) was grown in Gibco OptiMEM supplemented with 10% fetal bovine serum (FBS) and 1% penicillin-streptomycin. pEGFP-C1-Rab plasmids library, pEGFP-C1-Rab8a(Q67L), pEGFP-C1-Rab8a(T22N), pEGFP-C1-Rab11a(Q70L), pEGFP-C1-Rab11a(S25N) and pEGFP-C1-Rabin8, and pEGFP-C1-GRAB were prepared as described previously (Furusawa et al., 2017; Ishida et al., 2012; Matsui and Fukuda, 2011; Tsuboi and Fukuda, 2006). GFP-VAMP3 was a kind gift from Thierry Galli (Center of Psychiatry and Neuroscience, INSERM U894, Paris France). GFP MICAL1 and GFP MICAL-LI were a kind gift from Arnaud Echard (Institut Pasteur, Paris). The shRNA non-target control (SHC016-1EA), shRNA Rab8a (TRCN0000100422) and shRNA Rab11a (TRCN0000100344) were from Sigma Aldrich. ShRNA Rabin8 was prepared as described previously (Homma and Fukuda, 2016). Anti-Rabin8 was purified as described (Homma and Fukuda, 2016). Anti-Rab8a antibody (ab188574), Anti-Rab11a antibody (ab128913) and anti-VAMP3 antibody (ab2102) were from Abcam. GFP-vector and H2B-mCherry-vector were from AddGene. CAD cells were transiently transfected with Lipofectamine 2000 (Invitrogen) according to the manufacturer's instructions.

High-content screening of Rab-GTPases

Confluent CAD cells were mechanically detached and counted, and 5000 cells were plated for 6 h in 96-well plates (Greiner Bio-One). The 41 GFP-Rab GTPase plasmids were mixed with 10 μ l Opti-MEM, and 0.2 μ l Lipofectamine was mixed with 10 μ l Opti-MEM. After mixing these two compartments for 15 min, the transfection mixture was added to cells and 80 μ l additional complete medium was added to cells. After 16 h of transfection, cells were labeled with lipophilic tracer VybrantTM DiD (long-chain dialkylcarbocyanine) in complete medium for 30 min at 37°C and rinsed with PBS. 5000 CAD cells that had been transfected with H2B-mCherry were added to each well and co-cultured for 24 h. Cells were fixed with 4% PFA for 20 min at room temperature and labeled with HCS CellMaskTM Blue. Images were acquired with a 20 \times objective from Opera Phenix High Content Screening System (PerkinElmer). Fifty images of different fields from each well were acquired and analyzed using Cellprofiler (<http://cellprofiler.org/>).

Quantification of TNT-connected cells

Confluent CAD cells were mechanically detached and counted, and 300,000 cells were plated for 6 h in six-well plates. Cells were transfected with the appropriate plasmids. At 24 h post-transfection, cells were detached and counted, and 220,000 cells were plated for 16 h on Ibidi μ -dishes (Biovalley, France). At 16 h post-seeding, cells were fixed with fixative solution 1 (2% PFA, 0.05% glutaraldehyde and 0.2 M HEPES in PBS) for 20 min at 37°C, followed by a second 20 min fixation with fixative solution 2 (4% PFA and 0.2 M HEPES in PBS) at 37°C. The cells were gently washed with PBS and labeled with WGA-Alexa Fluor 594 (Sigma) (1:300 in PBS) for 20 min at room temperature, washed and sealed with Aqua-Polymount (Polysciences, Inc.). Cells were labeled with WGA-Alexa Fluor 594 for the plasma membrane and DAPI for the nucleus in all the experiments.

Image stacks (0.3 μ m) covering the whole cellular volume were acquired using a confocal microscope (Zeiss LSM 700) controlled by ZEN software. To evaluate the number of TNT-connected cells, manual analysis was performed for transfected cells with TNTs. The criterion for identifying TNTs was that a continuous connection could be found when moving along the stacks after removing the bottom three slices. The two cells connected by at least one continuous connection were marked as TNT-connected cells. Each experiment was performed at least in triplicate. Image analyses and

displays of raw data, such as Z-projections, were obtained using ICY software (Gousset et al., 2013).

Fluorescence image analysis to quantify the transfer of DiD-labeled vesicles

Confluent CAD cells were mechanically detached and counted, and 800,000 cells were plated for 6 h in T25 flasks. The cells were transfected with the appropriate GFP-tagged constructs for donor cells and H2B-mCherry for acceptor cells for 24 h in complete medium. The donor cells were labeled using a 333 nM solution of VybrantTM DiD in complete medium for 30 min at 37°C. Cells were then washed with PBS and 0.01% trypsin, resuspended in complete medium and counted. The labeled donor cells were mixed in a 1:1 ratio with H2B-transfected acceptor cells and plated at subconfluence (220,000 cells) on Ibidi μ -dishes (Biovalley, France) for 16 h at 37°C. Cells were fixed with 4% PFA. Cells were washed and sequentially stained for 30 min with a 1 μ g ml⁻¹ solution of HCS CellMaskTM Blue, which stains the entire cell volume (i.e. cytoplasm and nucleus). Samples were washed and sealed with Aqua-Poly/Mount (Polysciences, Inc.). The cells were imaged with an inverted confocal microscope (Zeiss LSM700) controlled by ZEN software. Quantification was carried out using ICY software (<http://icy.bioimageanalysis.org/>).

Flow cytometry to analyze the transfer of DiD-labeled vesicles

Confluent CAD cells were mechanically detached and counted, and 800,000 cells were plated for 6 h in T25 flasks. Cells were transfected with Lipofectamine 2000 (Invitrogen), according to the manufacturer's instructions, with the appropriate GFP-tagged constructs for donor cells and with H2B-mCherry for acceptor cells, for 24 h in complete medium. Donor cells were detached, counted and labeled with a 333 nM solution of VybrantTM DiD in complete medium for 30 min at 37°C. Cells were then washed with PBS and 0.01% trypsin, resuspended in complete medium and counted.

The labeled donor cells were mixed in a 1:1 ratio with H2B-mCherry-transfected acceptor cells and plated at subconfluence (120,000 cells per well) on 24-well plates for 16 h at 37°C. Each independent co-culture was performed in triplicate. To verify that the transfer of vesicles between cells is cell-cell dependent and not through secretion, two populations of cells were co-cultured with a Transwell insert (i.e. a filter; 0.4 μ m) that could separate two populations of cells but share the medium. Alternatively, the supernatant from donor cells after overnight culture was taken and added to acceptor cells for another 16 h of culture. Cells were then washed with PBS, mechanically detached from the dish by pipetting up and down with 500 μ l PBS and then passed through sterile 40-mm nylon cell strainers (BD FalconTM) in order to obtain single-cell suspensions. Cell suspensions were fixed with 500 μ l of 4% PFA (2% final solution). Flow cytometry data were acquired using an LSR Fortessa flow cytometer (BD Biosciences). GFP fluorescence was analyzed at 488 nm excitation wavelength, RFP and mCherry fluorescence were analyzed at 561 nm excitation wavelength and DiD fluorescence was analyzed at 640 nm excitation wavelength. Samples were analyzed at a high flow rate, corresponding to 200–400 events per second, and 10,000 events were acquired for each condition. Data were analyzed using FlowJo analysis software.

Quantification of vinculin-positive peripheral focal adhesion

For indirect immunofluorescence labeling of vinculin, 90,000 cells were plated for 16 h on Ibidi μ -dishes and then fixed in 4% PFA in PBS for 15 min at 37°C. Cell samples were quenched with 50 mM NH₄Cl for 15 min, then permeabilized with 0.01% saponin in PBS containing 2% BSA (w/v) for 20 min at 37°C. After a first 1-h incubation with mouse anti-vinculin antibody (V9264, Sigma) diluted 1:500 in PBS containing 0.01% saponin and 2% BSA (w/v), cells were thoroughly washed and incubated for 40 min with goat anti-mouse Alexa Fluor 488 (Invitrogen) diluted 1:500 in PBS containing 0.01% saponin and 2% BSA (w/v). Cells were washed and sequentially stained for 20 min with a 3.3 μ g μ l⁻¹ solution of WGA Alexa Fluor 647 nm conjugate, for 30 min with 1 μ g ml⁻¹ solution of HCS CellMaskTM Blue, which stains the entire cell volume (i.e. cytoplasm and nucleus), and for 5 min with a 0.2 μ g μ l⁻¹ solution of DAPI. Samples were

washed and sealed with Aqua-Poly/Mount (Polysciences, Inc.). The bottom of the cell (in contact with the plastic dish) was imaged with an inverted confocal microscope (Zeiss LSM700) controlled by ZEN software. Displayed images corresponded to stack projections. Only linear corrections were applied, using the software ImageJ. Vinculin-positive peripheral focal adhesion was automatically detected and counted using ICY software (<http://icy.bioimageanalysis.org/>).

Western blot

Cells transfected with shRNA were lysed in NP-40 lysis buffer (25 mM Tris, pH 7–8, 150 mM NaCl, 0.1% SDS, 0.5% sodium deoxycholate, 1% Triton X-100). Protein concentration in the cell lysate was quantified using a Bradford protein assay (Bio-Rad). Protein samples were incubated at 100°C for 5 min and electrophoresed on 10% SDS-polyacrylamide gels. Proteins were transferred to PVDF membranes (GE Healthcare Life Sciences). Membranes were blocked in 5% nonfat milk in Tris-buffered saline with 0.1% Tween 20 (Sigma) (TBS-T) for 1 h. Membranes were then incubated at 4°C with a primary antibody, rabbit anti-Rab8a, anti-Rab11a, anti-VAMP3 and anti-Rabin8 and mouse anti- α -tubulin (Sigma) or anti-rabbit GAPDH (Cell Signaling Technology) diluted in 5% nonfat milk overnight (1:500 and 1:10,000, respectively) then washed several times with TBS-T. After 1 h incubation with horseradish peroxidase conjugated with the respective IgG secondary antibody (1:10,000) (GE Healthcare Life Sciences), membranes were washed with TBS-T and protein bands on the membrane were detected using an ECL-Plus immunoblotting chemiluminescence system (GE Healthcare Life Sciences). Membranes were imaged using ImageQuant LAS 500TM camera (GE Healthcare Life Sciences).

Acknowledgements

The authors thank A. Echard (Institut Pasteur) and all C.Z. laboratory members for discussion and J. Y. Vargas, C. Brou, M. Henderson and D. Cordero-Cervantes for critical reading of the manuscript. We gratefully acknowledge the Imagopole–Citech of Institut Pasteur (Paris). We are also grateful for the financial support of Institut Pasteur (Paris).

Competing interests

The authors declare no competing or financial interests.

Author contributions

Conceptualization: S.Z., C.Z.; Methodology: S.Z., Y.K., C.Z.; Software: S.Z.; Validation: S.Z., S.B.; Formal analysis: S.Z., S.B.; Investigation: S.Z., S.B., S.S., Y.K., M.F.; Resources: S.Z.; Data curation: S.Z.; Writing - original draft: S.Z., S.B., M.F., C.Z.; Writing - review & editing: S.Z., S.B., M.F., C.Z.; Visualization: S.Z., C.Z.; Supervision: M.F., C.Z.; Project administration: C.Z.; Funding acquisition: C.Z.

Funding

This work was supported by the Agence Nationale de la Recherche (ANR 16 CE 16 0019 01 NEUROTUNN) and the EU Joint Programme on Neurodegenerative Diseases (JPND-NeuTARGETs-ANR-14-JPCD-0002-02) and by Equipe FRM (Fondation pour la Recherche Médicale) 2014 (DEQ 20140329557) to C.Z. S.Z. is supported by Ph.D. fellowships from the China Scholarship Council (201306170046) and by an Institute Carnot fellowship. S.B. is supported by JPND-NeuTARGETs-ANR-14-JPCD-0002-02 and INSERM (HTE201602).

Supplementary information

Supplementary information available online at <http://jcs.biologists.org/lookup/doi/10.1242/jcs.215889.supplemental>

References

- Abounit, S. and Zurzolo, C.** (2012). Wiring through tunneling nanotubes—from electrical signals to organelle transfer. *J. Cell Sci.* **125**, 1089–1098.
- Abounit, S., Delage, E. and Zurzolo, C.** (2015). Identification and characterization of tunneling nanotubes for intercellular trafficking. *Curr. Protoc. Cell Biol.* **67**, 12.10.1–21.
- Abounit, S., Bousset, L., Loria, F., Zhu, S., de Chaumont, F., Pieri, L., Olivo-Marin, J. C., Melki, R. and Zurzolo, C.** (2016a). Tunneling nanotubes spread fibrillar alpha-synuclein by intercellular trafficking of lysosomes. *EMBO J.* **35**, 2120–2138.
- Abounit, S., Wu, J. W., Duff, K., Victoria, G. S. and Zurzolo, C.** (2016b). Tunneling nanotubes: a possible highway in the spreading of tau and other prion-like proteins in neurodegenerative diseases. *Prion* **10**, 344–351.
- Arkwright, P. D., Luchetti, F., Tour, J., Roberts, C., Ayub, R., Morales, A. P., Rodríguez, J. J., Gilmore, A., Canonico, B., Papa, S. et al.** (2010). Fas stimulation of T lymphocytes promotes rapid intercellular exchange of death signals via membrane nanotubes. *Cell Res.* **20**, 72–88.
- Austefjord, M. W., Gerdes, H.-H. and Wang, X.** (2014). Tunneling nanotubes: Diversity in morphology and structure. *Commun. Integr. Biol.* **7**, e27934.
- Biran, A., Perelmutter, M., Gal, H., Burton, D. G. A., Ovadya, Y., Vadai, E., Geiger, T. and Krizhanovsky, V.** (2015). Senescent cells communicate via intercellular protein transfer. *Genes Dev.* **29**, 791–802.
- Bishai, E. A., Sidhu, G. S., Li, W., Dhillon, J., Bohil, A. B., Cheney, R. E., Hartwig, J. H. and Southwick, F. S.** (2013). Myosin-X facilitates Shigella-induced membrane protrusions and cell-to-cell spread. *Cell. Microbiol.* **15**, 353–367.
- Boehlke, C., Bashkurov, M., Buescher, A., Krick, T., John, A.-K., Nitschke, R., Walz, G. and Kuehn, E. W.** (2010). Differential role of Rab proteins in ciliary trafficking: Rab23 regulates smoothened levels. *J. Cell Sci.* **123**, 1460–1467.
- Bohil, A. B., Robertson, B. W. and Cheney, R. E.** (2006). Myosin-X is a molecular motor that functions in filopodia formation. *Proc. Natl. Acad. Sci. USA* **103**, 12411–12416.
- Bravo-Cordero, J. J., Cordani, M., Soriano, S. F., Díez, B., Muñoz-Agudo, C., Casanova-Acebes, M., Boullosa, C., Guadamillas, M. C., Ezkurdia, I., Gonzalez-Pisano, D. et al.** (2016). A novel high-content analysis tool reveals Rab8-driven cytoskeletal reorganization through Rho GTPases, calpain and MT1-MMP. *J. Cell Sci.* **129**, 1734–1749.
- Bukoreshtliev, N. V., Wang, X., Hodneland, E., Gurke, S., Barroso, J. F. V. and Gerdes, H.-H.** (2009). Selective block of tunneling nanotube (TNT) formation inhibits intercellular organelle transfer between PC12 cells. *FEBS Lett.* **583**, 1481–1488.
- Burtey, A., Wagner, M., Hodneland, E., Skafnesmo, K. O., Schoelermann, J., Mondragon, I. R., Espedal, H., Golebiewska, A., Niclou, S. P., Bjerkvig, R. et al.** (2015). Intercellular transfer of transferrin receptor by a contact-, Rab8-dependent mechanism involving tunneling nanotubes. *FASEB J.* **29**, 4695–4712.
- Campa, C. C. and Hirsch, E.** (2017). Rab11 and phosphoinositides: A synergy of signal transducers in the control of vesicular trafficking. *Adv. Biol. Regul.* **63**, 132–139.
- Carroll, K. S., Hanna, J., Simon, I., Krise, J., Barbero, P. and Pfeffer, S. R.** (2001). Role of Rab9 GTPase in facilitating receptor recruitment by TIP47. *Science* **292**, 1373–1376.
- Castillo-Romero, A., Leon-Avila, G., Wang, C. C., Perez Rangel, A., Camacho Nuez, M., Garcia Tovar, C., Ayala-Sumano, J. T., Luna-Arias, J. P. and Hernandez, J. M.** (2010). Rab11 and actin cytoskeleton participate in Giardia lamblia encystation, guiding the specific vesicles to the cyst wall. *PLoS Negl. Trop. Dis.* **4**, e697.
- Chen, W., Feng, Y., Chen, D. Y. and Wandinger-Ness, A.** (1998). Rab11 is required for trans-Golgi network to plasma membrane transport and a preferential target for GDP dissociation inhibitor. *Mol. Biol. Cell* **9**, 3241–3257.
- Cox, D., Lee, D. J., Dale, B. M., Calafat, J. and Greenberg, S.** (2000). A Rab11-containing rapidly recycling compartment in macrophages that promotes phagocytosis. *Proc. Natl. Acad. Sci. USA* **97**, 680–685.
- Davis, D. M. and Sowinski, S.** (2008). Membrane nanotubes: dynamic long-distance connections between animal cells. *Nat. Rev. Mol. Cell Biol.* **9**, 431–436.
- Delage, E., Cervantes, D. C., Penard, E., Schmitt, C., Syan, S., Disanza, A., Scita, G. and Zurzolo, C.** (2016). Differential identity of Filopodia and Tunneling Nanotubes revealed by the opposite functions of actin regulatory complexes. *Sci. Rep.* **6**, 39632.
- Deng, W. J., Wang, Y. Y., Gu, L., Duan, B. A., Cui, J., Zhang, Y. J., Chen, Y., Sun, S. X., Dong, J. and Du, J.** (2016). MICAL1 controls cell invasive phenotype via regulating oxidative stress in breast cancer cells. *BMC Cancer* **16**, 489.
- Diekmann, Y., Seixas, E., Gouw, M., Tavares-Cadete, F., Seabra, M. C. and Pereira-Leal, J. B.** (2011). Thousands of rab GTPases for the cell biologist. *PLoS Comput. Biol.* **7**, e1002217.
- Disanza, A., Bisi, S., Winterhoff, M., Milanese, F., Ushakov, D. S., Kast, D., Marighetti, P., Romet-Lemonne, G., Muller, H. M., Nickel, W. et al.** (2013). CDC42 switches IRSp53 from inhibition of actin growth to elongation by clustering of VASP. *EMBO J.* **32**, 2735–2750.
- Dustin, M. L., Chakraborty, A. K. and Shaw, A. S.** (2010). Understanding the structure and function of the immunological synapse. *Cold Spring Harb. Perspect. Biol.* **2**, a002311.
- Eva, R., Dassisti, E., Caswell, P. T., Dick, G., French-Constant, C., Norman, J. C. and Fawcett, J. W.** (2010). Rab11 and its effector Rab coupling protein contribute to the trafficking of beta 1 integrins during axon growth in adult dorsal root ganglion neurons and PC12 cells. *J. Neurosci.* **30**, 11654–11669.
- Finetti, F., Patrussi, L., Galgano, D., Cassioli, C., Perinetti, G., Pazour, G. J. and Baldari, C. T.** (2015). The small GTPase Rab8 interacts with VAMP-3 to regulate the delivery of recycling T-cell receptors to the immune synapse. *J. Cell Sci.* **128**, 2541–2552.
- Folliit, J. A., Li, L., Vucica, Y. and Pazour, G. J.** (2010). The cytoplasmic tail of fibrocystin contains a ciliary targeting sequence. *J. Cell Biol.* **188**, 21–28.
- Fremont, S., Hammich, H., Bai, J., Wioland, H., Klinkert, K., Rocancourt, M., Kikuti, C., Stroebel, D., Romet-Lemonne, G., Pylypenko, O. et al.** (2017).

- Oxidation of F-actin controls the terminal steps of cytokinesis. *Nat. Commun.* **8**, 1-16.
- Fukuda, M.** (2008). Regulation of secretory vesicle traffic by Rab small GTPases. *Cell. Mol. Life Sci.* **65**, 2801-2813.
- Furusawa, K., Asada, A., Urrutia, P., Gonzalez-Billault, C., Fukuda, M. and Hisanaga, S.** (2017). Cdk5 regulation of the GRAB-mediated Rab8-Rab11 cascade in axon outgrowth. *J. Neurosci.* **37**, 790-806.
- Gousset, K., Schiff, E., Langevin, C., Marjanovic, Z., Caputo, A., Browman, D. T., Chenouard, N., de Chaumont, F., Martino, A., Enninga, J. et al.** (2009). Prions hijack tunnelling nanotubes for intercellular spread. *Nat. Cell Biol.* **11**, 328-336.
- Gousset, K., Marzo, L., Commere, P.-H. and Zurzolo, C.** (2013). Myo10 is a key regulator of TNT formation in neuronal cells. *J. Cell Sci.* **126**, 4424-4435.
- Hanna, S. J., McCoy-Simandle, K., Miskolci, V., Guo, P., Cammer, M., Hodgson, L. and Cox, D.** (2017). The Role of Rho-GTPases and actin polymerization during Macrophage Tunneling Nanotube Biogenesis. *Sci. Rep.* **7**, 8547.
- Hase, K., Kimura, S., Takatsu, H., Ohmae, M., Kawano, S., Kitamura, H., Ito, M., Watarai, H., Hazelett, C. C., Yeaman, C. et al.** (2009). M-Sec promotes membrane nanotube formation by interacting with Ral and the exocyst complex. *Nat. Cell Biol.* **11**, 1427-1432.
- Hattula, K., Furuhielm, J., Arffman, A. and Peränen, J.** (2002). A Rab8-specific GDP/GTP exchange factor is involved in actin remodeling and polarized membrane transport. *Mol. Biol. Cell* **13**, 3268-3280.
- Hattula, K., Furuhielm, J., Tikkanen, J., Tanhuanpaa, K., Laakkonen, P. and Peränen, J.** (2006). Characterization of the Rab8-specific membrane traffic route linked to protrusion formation. *J. Cell Sci.* **119**, 4866-4877.
- Higgs, H. N. and Pollard, T. D.** (1999). Regulation of actin polymerization by Arp2/3 complex and WASp/Scar proteins. *J. Biol. Chem.* **274**, 32531-32534.
- Homma, Y. and Fukuda, M.** (2016). Rabin8 regulates neurite outgrowth in both GEF activity-dependent and -independent manners. *Mol. Biol. Cell* **27**, 2107-2118.
- Hutagalung, A. H. and Novick, P. J.** (2011). Role of Rab GTPases in membrane traffic and cell physiology. *Physiol. Rev.* **91**, 119-149.
- Ikedo, M., Ishida, O., Hinoi, T., Kishida, S. and Kikuchi, A.** (1998). Identification and characterization of a novel protein interacting with Ral-binding protein 1, a putative effector protein of Ral. *J. Biol. Chem.* **273**, 814-821.
- Ishida, M., Ohbayashi, N., Maruta, Y., Ebata, Y. and Fukuda, M.** (2012). Functional involvement of Rab1A in microtubule-dependent anterograde melanosome transport in melanocytes. *J. Cell Sci.* **125**, 5177-5187.
- Kadiu, I. and Gendelman, H. E.** (2011). Macrophage bridging conduit trafficking of HIV-1 through the endoplasmic reticulum and golgi network. *J. Proteome Res.* **10**, 3225-3238.
- Kimura, S., Yamashita, M., Yamakami-Kimura, M., Sato, Y., Yamagata, A., Kobashigawa, Y., Inagaki, F., Amada, T., Hase, K., Iwanaga, T. et al.** (2016). Distinct roles for the N- and C-terminal regions of M-Sec in plasma membrane deformation during tunnelling nanotube formation. *Sci. Rep.* **6**, 33548.
- Klöpffer, T. H., Kienle, N., Fasshauer, D. and Munro, S.** (2012). Untangling the evolution of Rab G proteins: implications of a comprehensive genomic analysis. *BMC Biol.* **10**, 71.
- Kobayashi, H., Etoh, K., Ohbayashi, N. and Fukuda, M.** (2014). Rab35 promotes the recruitment of Rab8, Rab13 and Rab36 to recycling endosomes through MICAL-L1 during neurite outgrowth. *Biol. Open* **3**, 803-814.
- Marzo, L., Gousset, K. and Zurzolo, C.** (2012). Multifaceted roles of tunneling nanotubes in intercellular communication. *Front. Physiol.* **3**, 72.
- Matsui, T. and Fukuda, M.** (2011). Small GTPase Rab12 regulates transferrin receptor degradation: Implications for a novel membrane trafficking pathway from recycling endosomes to lysosomes. *Cell Logist* **1**, 155-158.
- Nachury, M. V., Loktev, A. V., Zhang, Q., Westlake, C. J., Peränen, J., Merdes, A., Slusarski, D. C., Scheller, R. H., Bazan, J. F., Sheffield, V. C. et al.** (2007). A core complex of BBS proteins cooperates with the GTPase Rab8 to promote ciliary membrane biogenesis. *Cell* **129**, 1201-1213.
- Nielsen, E., Christoforidis, S., Uttenweiler-Joseph, S., Miaczynska, M., Dewitte, F., Wilm, M., Hoflack, B. and Zerial, M.** (2000). Rabenosyn-5, a novel Rab5 effector, is complexed with hVPS41 and recruited to endosomes through a FYVE finger domain. *J. Cell Biol.* **151**, 601-612.
- Onfelt, B., Nedvetzki, S., Benninger, R. K. P., Purbhoo, M. A., Sowinski, S., Hume, A. N., Seabra, M. C., Neil, M. A. A., French, P. M. W. and Davis, D. M.** (2006). Structurally distinct membrane nanotubes between human macrophages support long-distance vesicular traffic or surfing of bacteria. *J. Immunol.* **177**, 8476-8483.
- Patrussi, L. and Baldari, C. T.** (2016). The Rab GTPase Rab8 as a shared regulator of ciliogenesis and immune synapse assembly: from a conserved pathway to diverse cellular structures. *Small GTPases* **7**, 16-20.
- Peränen, J.** (2011). Rab8 GTPase as a regulator of cell shape. *Cytoskeleton (Hoboken)* **68**, 527-539.
- Rahajeng, J., Giridharan, S. S. P., Cai, B. S., Naslavsky, N. and Caplan, S.** (2012). MICAL-L1 is a tubular endosomal membrane hub that connects Rab35 and Arf6 with Rab8a. *Traffic* **13**, 82-93.
- Ramalho, J. S., Anders, R., Jaissle, G. B., Seeliger, M. W., Huxley, C. and Seabra, M. C.** (2002). Rapid degradation of dominant-negative Rab27 proteins in vivo precludes their use in transgenic mouse models. *BMC Cell Biol.* **3**, 26.
- Ramel, D., Wang, X., Laflamme, C., Montell, D. J. and Emery, G.** (2013). Rab11 regulates cell-cell communication during collective cell movements. *Nat. Cell Biol.* **15**, 317-324.
- Reichert, D., Scheinpflug, J., Karbanova, J., Freund, D., Bornhauser, M. and Corbeil, D.** (2016). Tunneling nanotubes mediate the transfer of stem cell marker CD133 between hematopoietic progenitor cells. *Exp. Hematol.* **44**, 1092-1112 e2.
- Roland, J. T., Kenworthy, A. K., Peranen, J., Caplan, S. and Goldenring, J. R.** (2007). Myosin Vb interacts with Rab8a on a tubular network containing EHD1 and EHD3. *Mol. Biol. Cell* **18**, 2828-2837.
- Roland, J. T., Bryant, D. M., Datta, A., Itzen, A., Mostov, K. E. and Goldenring, J. R.** (2011). Rab GTPase-Myo5B complexes control membrane recycling and epithelial polarization. *Proc. Natl. Acad. Sci. USA* **108**, 2789-2794.
- Rowe, R. K., Suszko, J. W. and Pekosz, A.** (2008). Roles for the recycling endosome, Rab8, and Rab11 in hantavirus release from epithelial cells. *Virology* **382**, 239-249.
- Rustom, A., Saffrich, R., Markovic, I., Walther, P. and Gerdes, H. H.** (2004). Nanotubular highways for intercellular organelle transport. *Science* **303**, 1007-1010.
- Sanchez, V., Villalba, N., Fiore, L., Luzzani, C., Miriuka, S., Boveris, A., Gelpi, R. J., Brusco, A. and Poderoso, J. J.** (2017). Characterization of tunneling nanotubes in Wharton's jelly mesenchymal stem cells: an intercellular exchange of components between neighboring cells. *Stem Cell Rev.* **13**, 491-498.
- Sato, T., Iwano, T., Kunii, M., Matsuda, S., Mizuguchi, R., Jung, Y., Hagiwara, H., Yoshihara, Y., Yuzaki, M., Harada, R. et al.** (2014). Rab8a and Rab8b are essential for several apical transport pathways but insufficient for ciliogenesis. *J. Cell Sci.* **127**, 422-431.
- Schafer, C., Born, S., Mohl, C., Houben, S., Kirchgessner, N., Merkel, R. and Hoffmann, B.** (2010). The key feature for early migratory processes: Dependence of adhesion, actin bundles, force generation and transmission on filopodia. *Cell Adh. Migr.* **4**, 215-225.
- Sharma, M., Giridharan, S. S. P., Rahajeng, J., Naslavsky, N. and Caplan, S.** (2009). MICAL-L1 links EHD1 to tubular recycling endosomes and regulates receptor recycling. *Mol. Biol. Cell* **20**, 5181-5194.
- Sherer, N. M. and Mothes, W.** (2008). Cytonemes and tunneling nanotubes in cell-cell communication and viral pathogenesis. *Trends Cell Biol.* **18**, 414-420.
- Shin, H.-W., Hayashi, M., Christoforidis, S., Lacas-Gervais, S., Hoepfner, S., Wenk, M. R., Modregger, J., Uttenweiler-Joseph, S., Wilm, M., Nystuen, A. et al.** (2005). An enzymatic cascade of Rab5 effectors regulates phosphoinositide turnover in the endocytic pathway. *J. Cell Biol.* **170**, 607-618.
- Shirane, M. and Nakayama, K. I.** (2006). Protrudin induces neurite formation by directional membrane trafficking. *Science* **314**, 818-821.
- Simonsen, A., Lippe, R., Christoforidis, S., Gaullier, J.-M., Brech, A., Callaghan, J., Toh, B.-H., Murphy, C., Zerial, M. and Stenmark, H.** (1998). EEA1 links PI(3)K function to Rab5 regulation of endosome fusion. *Nature* **394**, 494-498.
- Sowinski, S., Jolly, C., Berninghausen, O., Purbhoo, M. A., Chauveau, A., Köhler, K., Öddos, S., Eissmann, P., Brodsky, F. M., Hopkins, C. et al.** (2008). Membrane nanotubes physically connect T cells over long distances presenting a novel route for HIV-1 transmission. *Nat. Cell Biol.* **10**, 211-219.
- Stenmark, H.** (2009). Rab GTPases as coordinators of vesicle traffic. *Nat. Rev. Mol. Cell Biol.* **10**, 513-525.
- Takahashi, S., Kubo, K., Waguri, S., Yabashi, A., Shin, H.-W., Katoh, Y. and Nakayama, K.** (2012). Rab11 regulates exocytosis of recycling vesicles at the plasma membrane. *J. Cell Sci.* **125**, 4049-4057.
- Takano, T., Tomomura, M., Yoshioka, N., Tsutsumi, K., Terasawa, Y., Saito, T., Kawano, H., Kamiguchi, H., Fukuda, M. and Hisanaga, S.** (2012). LMTK1/AATYK1 is a novel regulator of axonal outgrowth that acts via Rab11 in a Cdk5-dependent manner. *J. Neurosci.* **32**, 6587-6599.
- Tsuboi, T. and Fukuda, M.** (2006). Rab3A and Rab27A cooperatively regulate the docking step of dense-core vesicle exocytosis in PC12 cells. *J. Cell Sci.* **119**, 2196-2203.
- van Weert, A. W., Geuze, H. J., Groothuis, B. and Stoorvogel, W.** (2000). Primaquine interferes with membrane recycling from endosomes to the plasma membrane through a direct interaction with endosomes which does not involve neutralisation of endosomal pH nor osmotic swelling of endosomes. *Eur. J. Cell Biol.* **79**, 394-399.
- Victoria, G. S. and Zurzolo, C.** (2017). The spread of prion-like proteins by lysosomes and tunneling nanotubes: implications for neurodegenerative diseases. *J. Cell Biol.* **216**, 2633-2644.
- Villarreal-Campos, D., Bronfman, F. C. and Gonzalez-Billault, C.** (2016). Rab GTPase signaling in neurite outgrowth and axon specification. *Cytoskeleton (Hoboken)* **73**, 498-507.
- Wang, Y., Cui, J., Sun, X. and Zhang, Y.** (2011). Tunneling-nanotube development in astrocytes depends on p53 activation. *Cell Death Differ.* **18**, 732-742.
- Wang, J., Ren, J., Wu, B., Feng, S., Cai, G., Tuluc, F., Peränen, J. and Guo, W.** (2015). Activation of Rab8 guanine nucleotide exchange factor Rabin8 by ERK1/2 in response to EGF signaling. *Proc. Natl. Acad. Sci. USA* **112**, 148-153.

- Westlake, C. J., Baye, L. M., Nachury, M. V., Wright, K. J., Ervin, K. E., Phu, L., Chalouni, C., Beck, J. S., Kirkpatrick, D. S., Slusarski, D. C. et al.** (2011). Primary cilia membrane assembly is initiated by Rab11 and transport protein particle II (TRAPP II) complex-dependent trafficking of Rabin8 to the centrosome. *Proc. Natl. Acad. Sci. USA* **108**, 2759-2764.
- Wu, X. S., Rao, K., Zhang, H., Wang, F., Sellers, J. R., Matesic, L. E., Copeland, N. G., Jenkins, N. A. and Hammer, J. A. III.** (2002). Identification of an organelle receptor for myosin-Va. *Nat. Cell Biol.* **4**, 271-278.
- Wu, S. Y., Mehta, S. Q., Pichaud, F., Bellen, H. J. and Quioco, F. A.** (2005). Sec15 interacts with Rab11 via a novel domain and affects Rab11 localization in vivo. *Nat. Struct. Mol. Biol.* **12**, 879-885.
- Zhang, X. M., Walsh, B., Mitchell, C. A. and Rowe, T.** (2005). TBC domain family, member 15 is a novel mammalian Rab GTPase-activating protein with substrate preference for Rab7. *Biochem. Biophys. Res. Commun.* **335**, 154-161.
- Zhao, Y. T., Liu, J. L., Yang, C. S., Capraro, B. R., Baumgart, T., Bradley, R. P., Ramakrishnan, N., Xu, X. W., Radhakrishnan, R., Svitkina, T. et al.** (2013). Exo70 generates membrane curvature for morphogenesis and cell migration. *Dev. Cell* **26**, 266-278.
- Zhen, Y. and Stenmark, H.** (2015). Cellular functions of Rab GTPases at a glance. *J. Cell Sci.* **128**, 3171-3176.
- Zhu, H., Xue, C., Xu, X., Guo, Y., Li, X., Lu, J., Ju, S., Wang, Y., Cao, Z. and Gu, X.** (2016). Rab8a/Rab11a regulate intercellular communications between neural cells via tunneling nanotubes. *Cell Death Dis.* **7**, e2523.
- Zhu, S., Abounit, S., Korth, C. and Zurzolo, C.** (2017). Transfer of disrupted-in-schizophrenia 1 aggregates between neuronal-like cells occurs in tunnelling nanotubes and is promoted by dopamine. *Open Biol.* **7**, 160328.

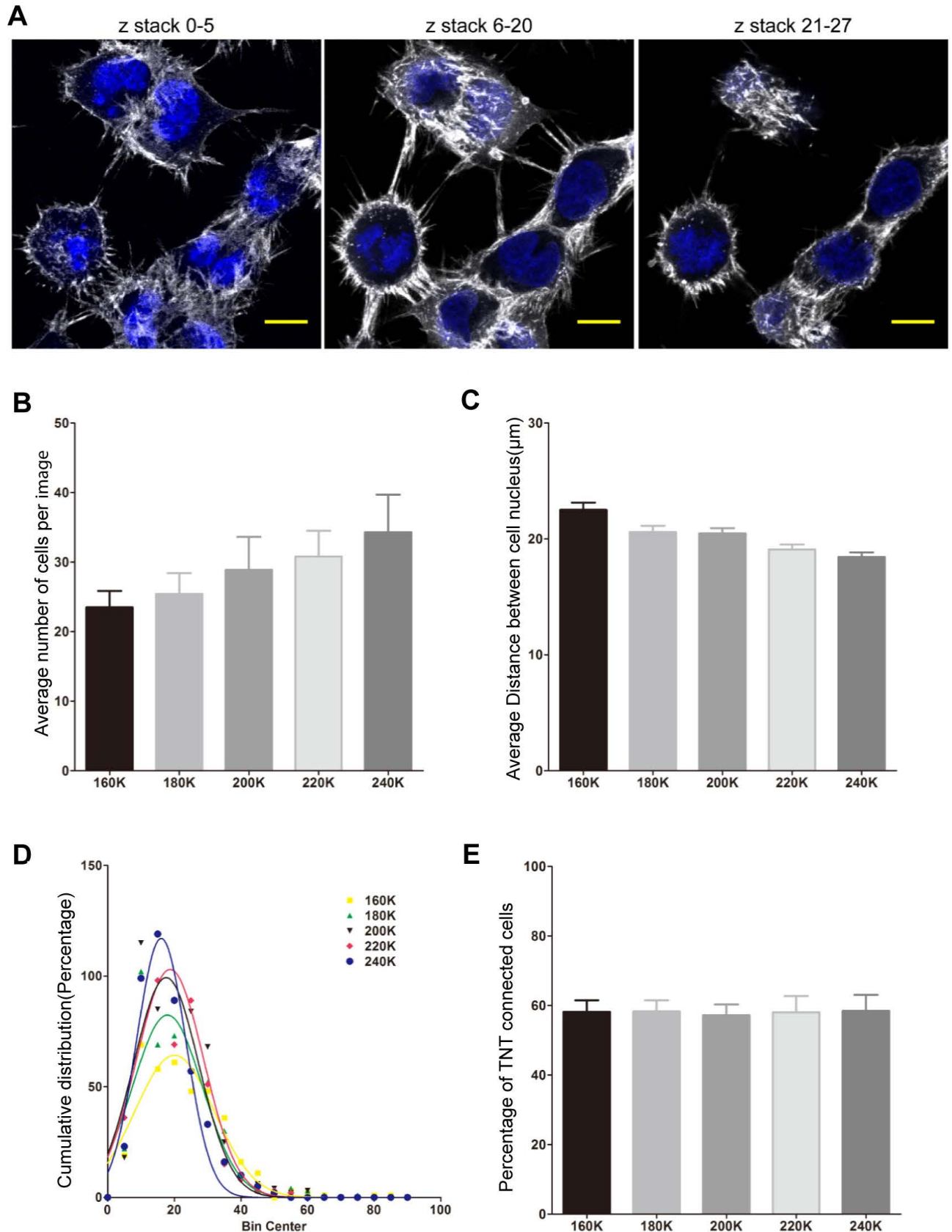


Fig. S1. The percentage of TNT connected cells does not change within a range of cell distance.

A. Representative confocal images of TNT formation between CAD cells. Images were acquired in 27 stacks, TNTs were present from stack 6 to stack 20. WGA-Alexa594 (white) was used to label cell plasma membrane and DAPI (blue) was used to label the nucleus. (Scale bar=10μm). **B.** Average number of CADs cells per images when 160K to 240K cells were plated (160K=23.77±1.39,180K=25.70±1.77,200K=29.21±2.769,220K=31.16±2.163,240K=34.70±3.149) **C.** Average distance between two cell nuclei from conditions as in (B) in mm(160K=22.51±0.62,180K=20.60±0.53,200K=20.49±0.43,220K=19.10±0.42,240K=18.44±0.40). **D.** Cumulative distribution of cell nuclear distance from conditions in (B). **E.** Bar graph representing average percentage of TNT connected cells from experiment described in (B) (160K=58.62±1.9 ,180K=58.75±1.91,200K=57.62±1.87,220K=58.49±2.72,240K=58.91±2.72)

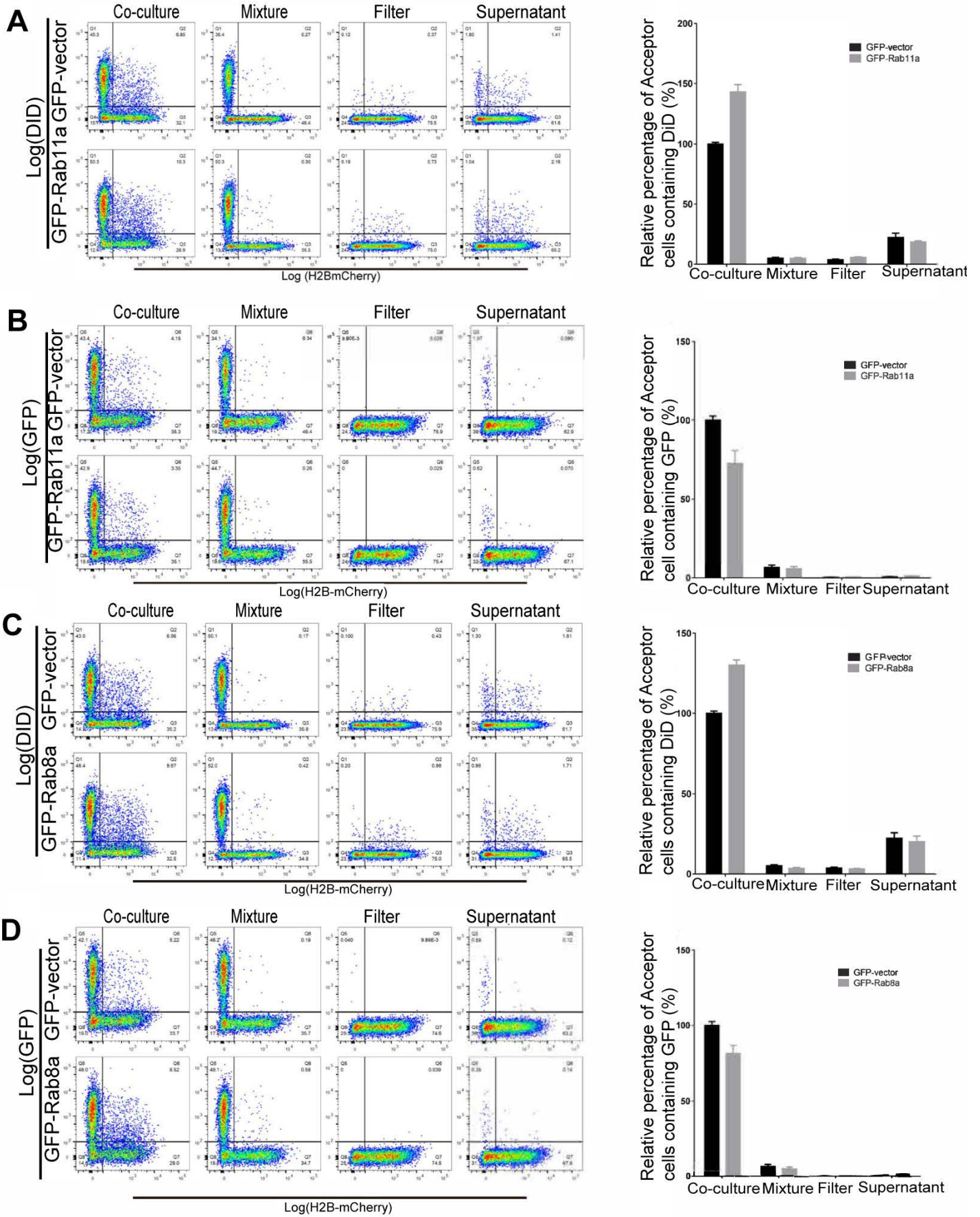


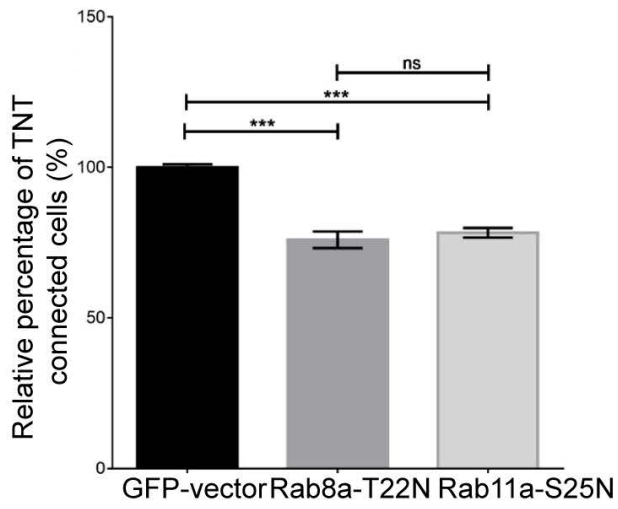
Fig. S2. DiD-labeled vesicles transfer between cells overexpressing Rab11a or Rab8a is mediated by cell-to-cell contact. A. Left panel, Raw data (dot plots) from a representative experiment showing the transfer of DiD-labeled vesicles to the acceptor cells population (H2B-mCherry) from mixture, co-culture with filter GFP-vector or GFP-Rab11a, coculture with/ without filter and supernatant between donor cells transfected with GFP-vector or GFP-Rab11a and acceptor cells. Right panel, Bar graph representing relative percentage of DiD positive acceptor cells by flow cytometry from conditions indicated in left panel mixture GFP-vector=5.03±0.67 or GFP-Rab11a=4.186±0.76, co-culture with filter GFP-vector=3.66±0.58, GFP-Rab11a=5.58±0.57 coculture without filter GFP-vector=100.0±1.4 or GFP-Rab11a=143.1±6.02 and supernatant GFP-vector=22.2±3.14 or GFP-Rab11a= 18.46±0.95

B. Left panel, Raw data (dot plots) from a representative experiment showing the transfer of GFP protein to the acceptor cells population (H2B-mCherry) from mixture, co-culture without filter with filter, and supernatant between donor cells transfected with GFP-vector or GFP-Rab11a and acceptor cells. Right panel shows bar graph representing relative percentage of GFP protein positive acceptor cells by flow cytometry from conditions indicated in left panel for mixture (GFP-vector=6.5±2.25 GFP-Rab11a=5.37±1.38), co-culture with filter (GFP-vector=0.35 ±0.17, GFP-Rab11a=0.44±0.08), coculture without filter (GFP-vector=100±3.84, GFP-Rab11a =72.64± 8.26) and supernatant (GFP-vector=0.85±0.21, GFP-Rab11a=1.13 ±0.12).

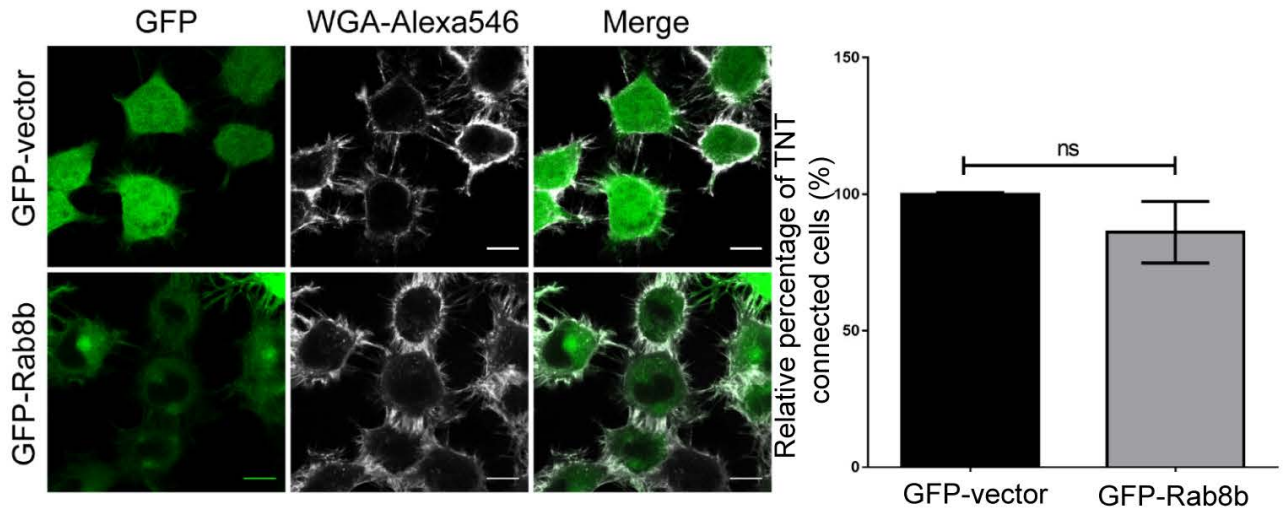
C. Left panel, Raw data (dot plots) from a representative experiment showing the transfer of DiD-labeled vesicles to the acceptor cells population (H2BmCherry) from mixture, co-culture (with/without filter) and supernatant between donor cells transfected with GFP-vector or GFP-Rab8a and acceptor cells. Right panel, Bar graph representing relative percentage of DiD positive acceptor cells by flow cytometry from conditions indicated in left panel for mixture GFP-vector=5.03±0.67 or GFP-Rab8a=3.46±0.6, co-culture with filter GFP-vector=3.6±0.58, GFP-Rab8a =3.193 coculture without filter GFP-vector=100.0±1.4 or GFP-Rab8a=130.1±3.23 and supernatant (GFP-vector=22.2±3.14 or GFP-Rab8a= 20.04±3.6).

D. Left panel, Raw data (dot plots) from a representative experiment showing the transfer of GFP protein to the acceptor cells population (H2B-mCherry) from mixture coculture with filter coculture without filter and supernatant between donor cells transfected with GFP-vector or GFP-Rab8a and acceptor cells. Right panel, Bar graph representing relative percentage of GFP protein positive acceptor cells by flow cytometry from conditions indicated in left panel for mixture (GFP-vector=9.09± 1.25, GFP-Rab8a=4.95±1.2), co-culture without filter (GFP-vector=100± 3.764 GFP-Rab8a= 81.64±5.40) with filter (GFP-vector=0.32±0.18, GFP-Rab8a=0.54±0.11), and supernatant (GFP-vector=0.57±0.29, GFP-Rab8a=0.54 ±0.11). Data represent the mean ± s.e.m of at least 3 independent experiments in triplicate setting

A



B



C

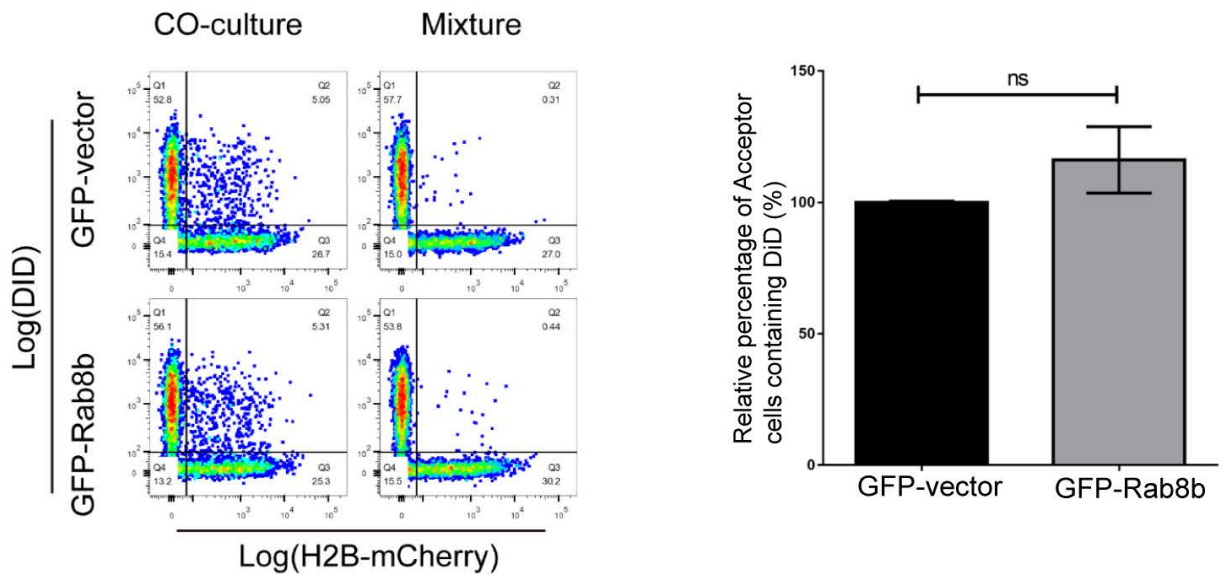


Fig.S3. Overexpression of inactive mutants of Rab11a and Rab8a for 52 hours significantly decreased the number of TNT-connected cells and Rab8b has no role in the TNT formation.

A. Bar graph showing relative percentage of TNT connected cells after transfection with either GFP-vector, GFP-Rab8a-T22N and Rab11a-S25N for 52hr (GFP-vector= 100 ± 0.577 , GFP-Rab8a-T22N= 75.94 ± 1.60 and Rab11a-S25N= 78.29 ± 0.92). The data represents the mean \pm s.e.m, of at least 3 independent experiments (ns, no significant; ***, $p < 0.001$ by One-way ANOVA with Tukey's multiple comparison post test). B. Left panel show representative confocal images of TNT connected cells after transfection with GFP-vector and GFP-Rab8b. Right panel is showing bar graph of relative percentage of the TNT-connected cells from the experiment described in the left panel (GFP-vector = 100.0 ± 0.5774 , GFP-Rab8b= 86.05 ± 11.27), the graph shows mean \pm s.e.m from three independent experiments (ns, no significant by Unpaired t test) C. Left panel shows the dot plot of the flow cytometry analysis of DiD transfer between donor cells overexpressing GFP-vector or GFP-Rab8b and acceptor cells expressing H2Bmcherry(GFP-vector= 100.0 ± 0.5774 , GFP-Rab8b= 116.2 ± 12.67). Right panel shows bar graph of the relative percentage of the acceptor cells with DiD. Data shows mean \pm s.e.m from three independent experiments (ns, no significant by unpaired student t test).

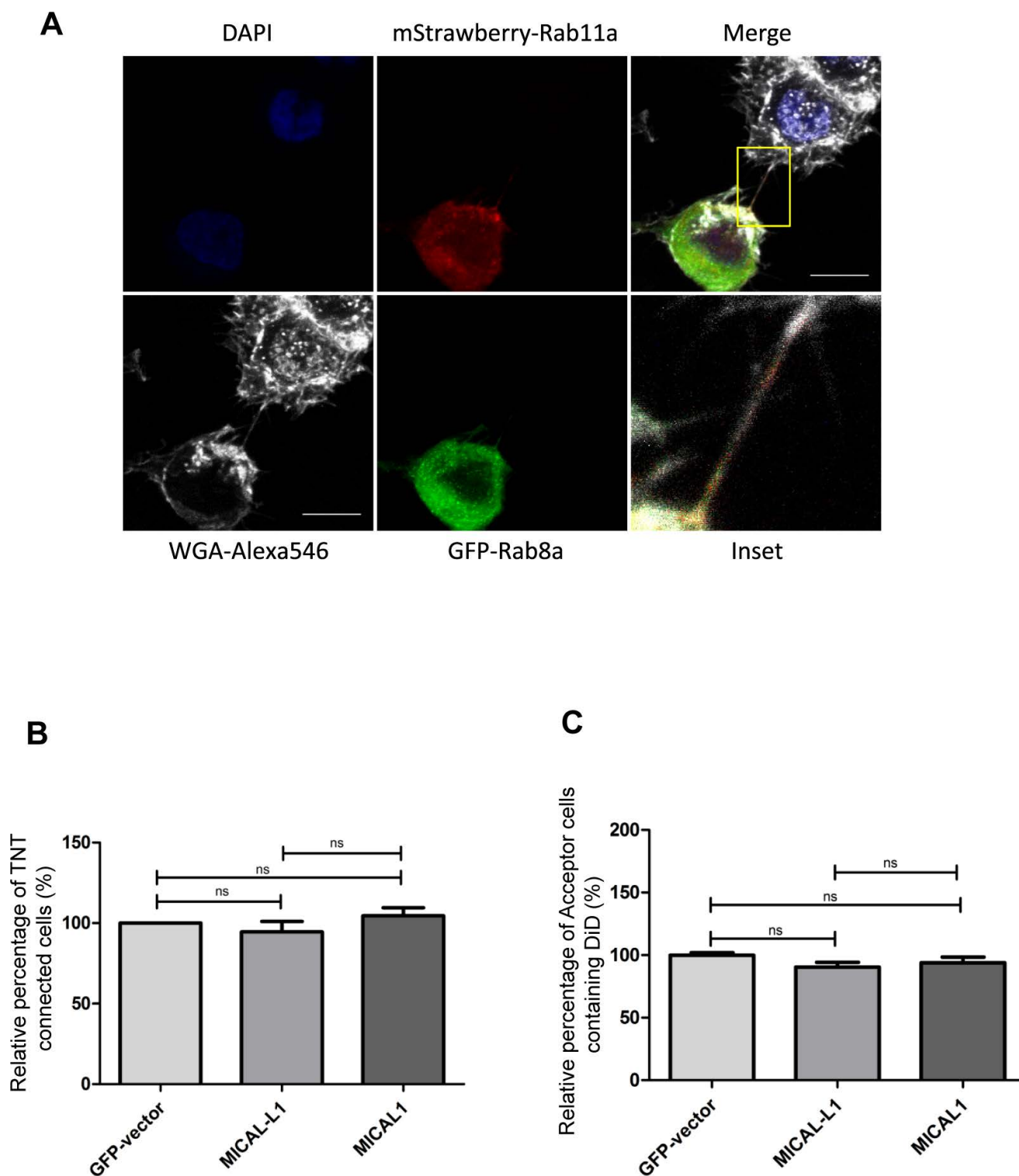


Fig.S4 Rabs do not colocalise on TNT and MICAL1 and MICAL-L1 has no effect on TNT formation: A Images show cells cotransfected with GFP-Rab8a(green) and mStrawberry-Rab11a(red). The DAPI (blue) and WGA-Alexa 594(white) was used to label the nucleus and cell membrane respectively. Inset shows the magnification of the region marked with yellow box from merge. (Scale bar =10µm) B. Bar graph representing the relative percentage of TNT-connected cells transfected with GFP-Vector, GFP-MICAL-L1, GFP-MICAL1. (GFP-Vector= 100±1.90, GFP-MICAL-L1= 90.46±3.75, GFP-MICAL1= 93.86±4.57) C. Bar graph showing the relative percentage of acceptor cells containing DiD labeled vesicles from the co-cultures, in which the donor cells were transfected with either GFP-Vector, GFP-MICAL-L1, GFP-MICAL1 and labeled with DiD. All the above bar graphs show mean ± s.e.m from three independent experiments (GFP-Vector= 100±0.00, GFP-MICAL-L1= 94.51±6.49, GFP-MICAL1= 104.5±4.98) (ns, no significant by One-way ANOVA with Tukey's multiple comparison post test).

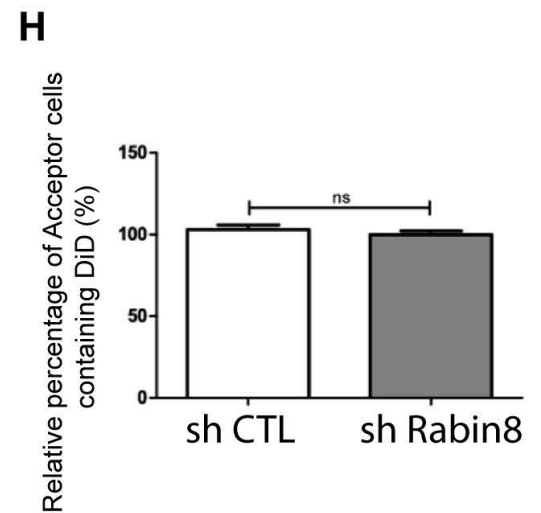
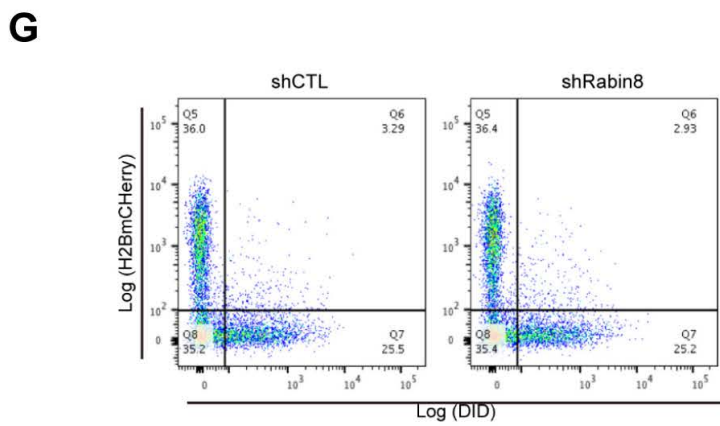
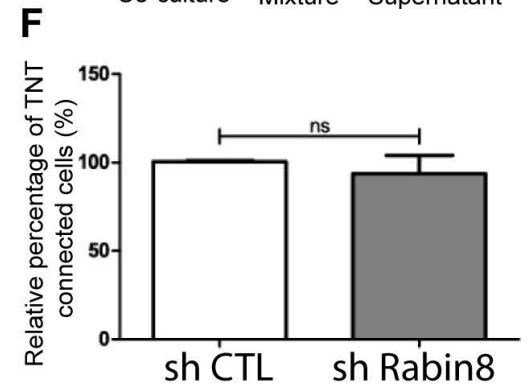
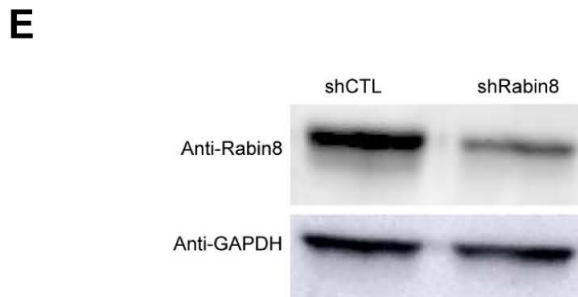
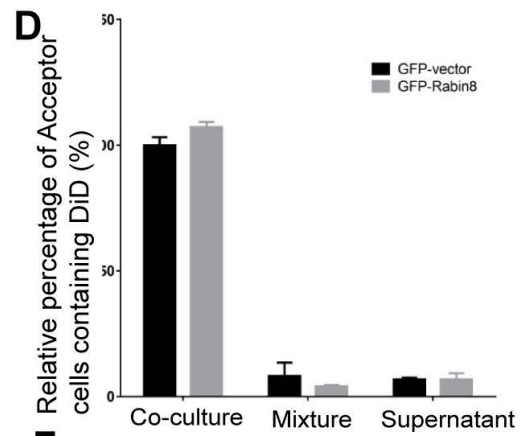
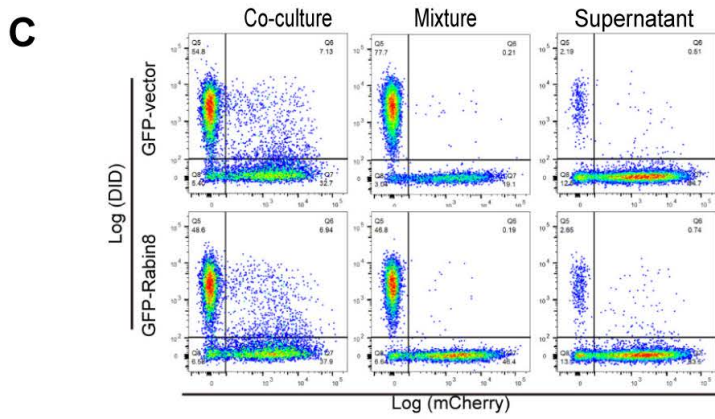
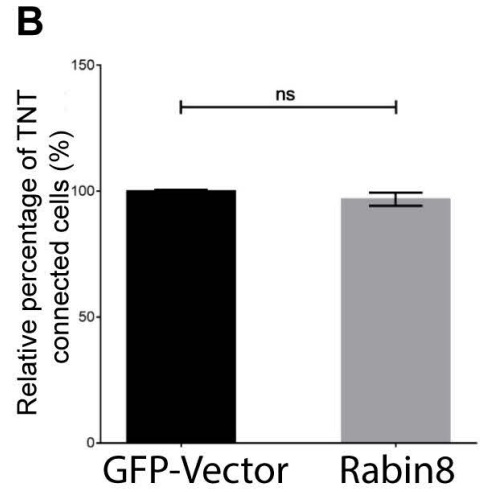
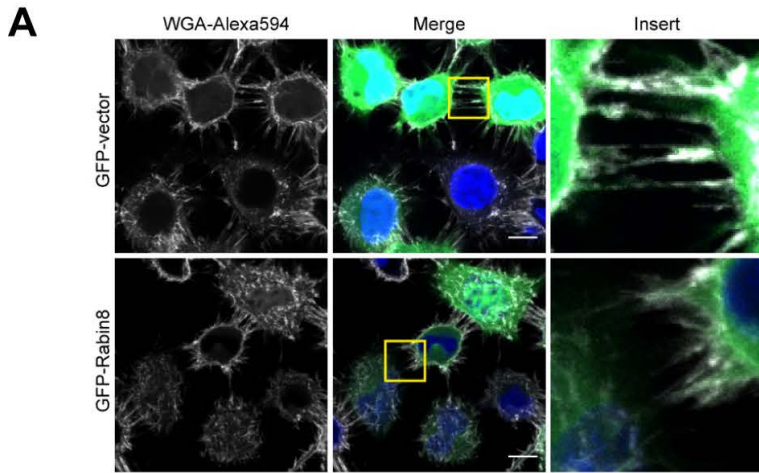
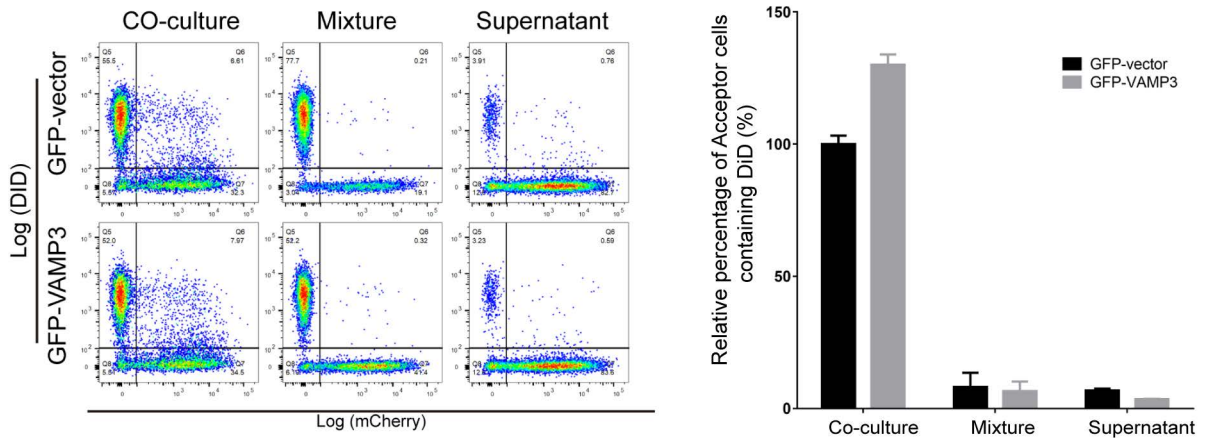


Fig.S5. Rabin8 has no effect on the number of TNT-connected cells and vesicle transfer between cells. A. Representative confocal images of TNT connected cells transfected with GFP vector or GFP-Rabin8. Inserts are enlargements of the framed region in merge panel. WGAAlexa594 (white) was used to label cell plasma membrane to show TNT between cells. (Scale bar=10 μ m). B. Bar graph showing relative percentage of TNT connected cells transfected with GFP-vector or GFP-Rabin8(GFP-vector=100 \pm 0.57, GFP-Rabin8=96.80 \pm 2.60). Data shows mean \pm s.e.m from three independent experiments (ns, no significant; by unpaired t test). C. Raw data (dot plots) from a representative experiment showing the transfer of DiD labeled vesicles to the acceptor cells population (H2B-mCherry) from co-culture, mixture and supernatant between donor cells transfected with GFP-vector or GFP-Rabin8 and acceptor cells by flow cytometry. D. Bar graph showing relative percentage of DiD positive acceptor cells from the experiment described in (C) (GFP-vector or GFP-Rabin8). Data represent the mean \pm s.e.m of three independent experiments in triplicate setting (ns, no significant; by unpaired student t test). E. Western blot analysis of extracts from cells transfected for 48h with ShRNA non-targeting (CTL) or targeting Rabin8 and GAPDH as loading control. F. Bar graph showing quantification of relative percentage of TNT connected cells transfected with ShCTL+GFP-vector or ShRabin8+GFP (ShCTL+GFP-vector= 100.5 \pm 0.5, ShRabin8+GFP= 93.74 \pm 10.37). Data shows mean \pm s.e.m from two independent experiment (ns, no significant; by unpaired student t test). G. Raw data (dot plots) from a representative experiment showing the transfer of DiD labeled vesicles to the acceptor cells population (H2B-mCherry) from co-culture between ShCTL+GFPvector and shRabin8+GFP-vector transfected donor cells and acceptor cells. H. Bar graph showing relative percentage DiD positive acceptor cells from the experiment described in (G) (ShCTL+GFPvector= 100.0 \pm 0.57, shRabin8+GFP-vector= 100.2 \pm 2.09). Data shows mean \pm s.e.m (ns, no significant; by unpaired t test) from one experiment performed in triplicate.)

A



B

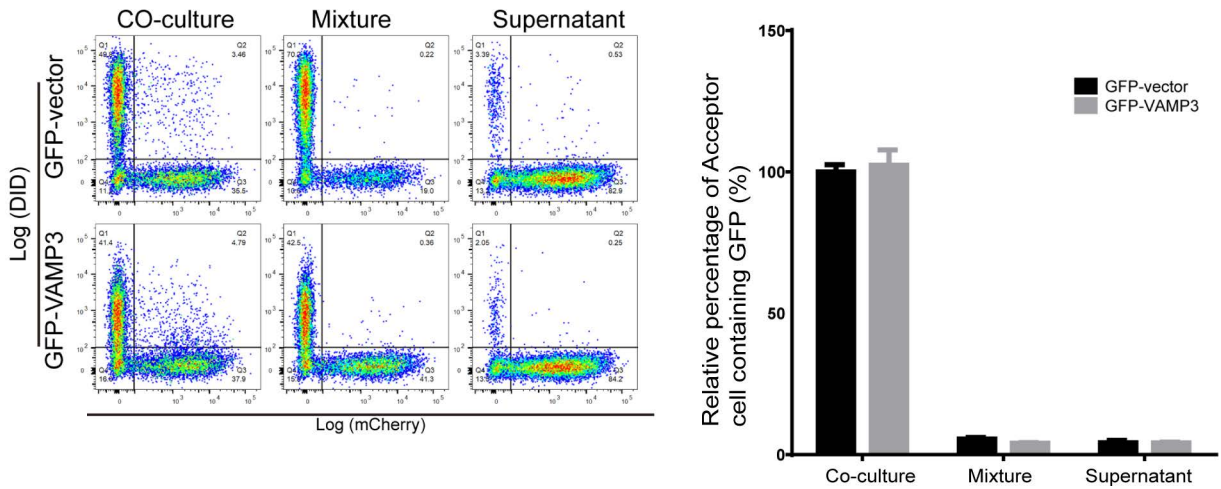


Fig. S6. DiD labeled vesicles transfer between cells affected by VAMP3 overexpression was mediated by cell-to-cell contact. A. Left panel, Raw data (dot plots) from a representative experiment showing the transfer of DiD labeled vesicles to the acceptor cells population (H2BmCherry) from co-culture, mixture, and supernatant between donor cells transfected with GFPvector or GFP-VAMP3 and acceptor cells, was analyzed by flow cytometry. Right panel, bar graph showing the relative percentage of DiD positive acceptor cells from the experiment described in the left panel (coculture GFPvector=100.0±1.5 or GFP- VAMP3=127.8±3.19 mixture GFPvector=4.5±1.38 GFP- VAMP3=4.15±1.18 supernatant GFPvector=3.18±0.01 GFP- VAMP3=3.7±0.74) Data represent the mean ± s.e.m. of at least 3 independent experiments in triplicates. B. Left panel, Raw data (dot plots) from a representative experiment showing the transfer of GFP-Vector or GFP-VAMP3 protein to the acceptor cells population (H2B-mCherry) from mixture, co-culture (with/without filter) and supernatant between GFP-vector or GFP-VAMP3 transfected donor cells and acceptor cells and analyzed by flow cytometry. Right panel, Bar graph showing relative percentage of DiD positive acceptor cells from the experiment described in the left panel. Data represent the mean ± s.e.m. of at least 3 independent experiments in triplicates.

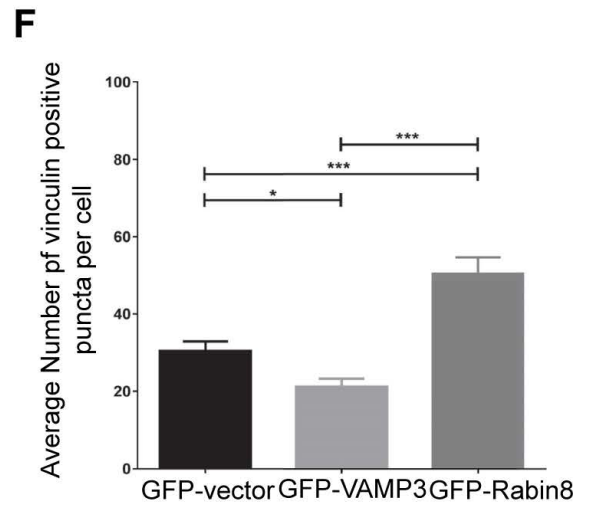
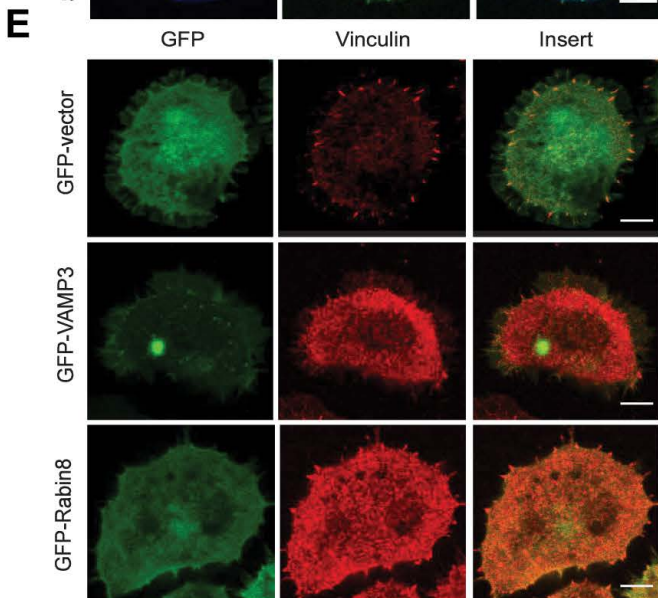
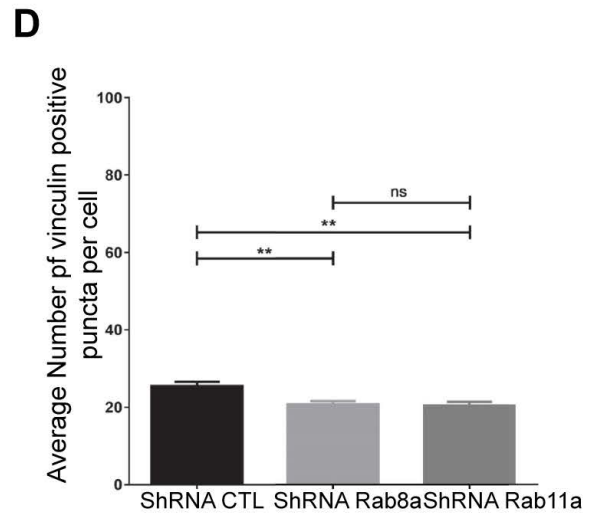
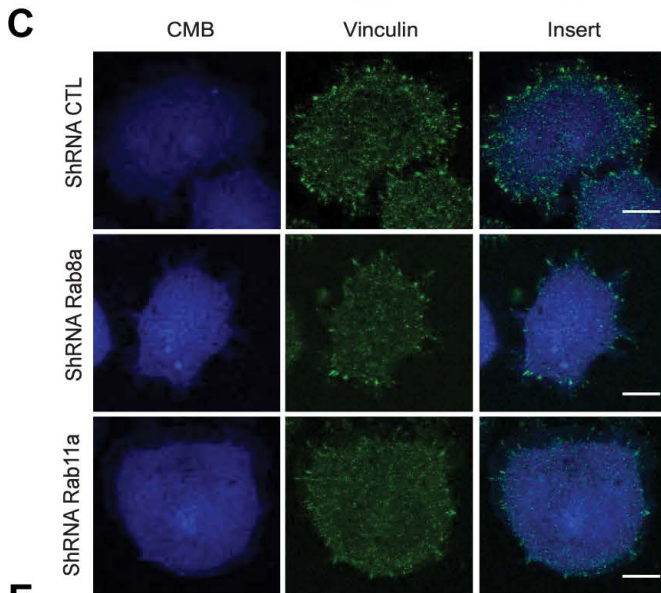
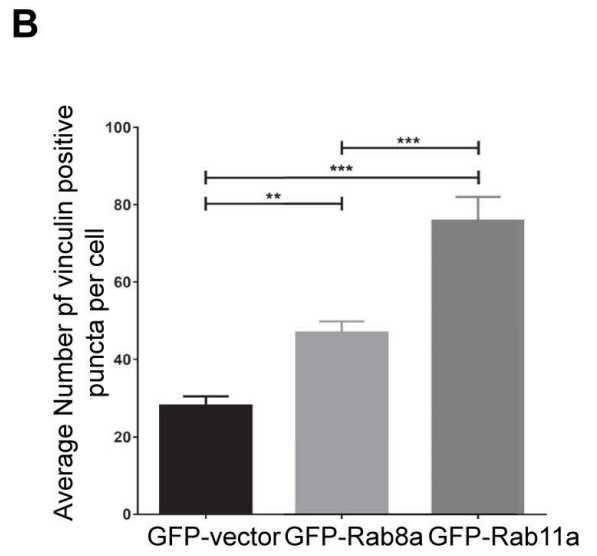
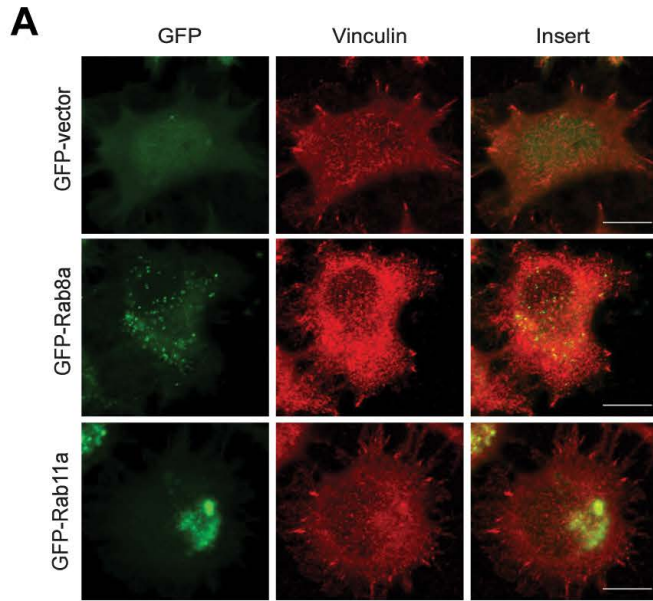


Fig. S7. Rab8a and Rab11a promote attached filopodia formation.

A. Representative confocal images of cells transfected with either GFP- vector, GFP-Rab8a or GFP-Rab11a. Cells were immunostained with anti-vinculin antibody (red). B. The bar graph represents the average number of vinculin positive puncta per cell from the experiment described in (A) (GFP- vector= 29.26 ± 1.91 , GFP-Rab8a= 40.84 ± 2.43 or GFP-Rab11a= 67.59 ± 5.87) C. Representative confocal images of cells transfected with either ShCTL, ShRab8a or ShRab11a. Cells were immunostained with anti-vinculin antibody (Green) and stained with HCS CellMaskTM. Quantification of average number of vinculin positive puncta per cell of the experiment described in (C) (ShCTL= 28.11 ± 1.25 , ShRab8a= 20.78 ± 0.84 , ShRab11a= 23.11 ± 0.87). E. Representative confocal images of cells transfected with either GFP-vector, GFPVAMP3 or GFP-Rabin8. Cells were immunostained with anti-vinculin antibody (Red). Representation of the average number of vinculin positive puncta per cell from the experiment described in (E) (GFP-vector= 30.52 ± 2.40 , GFPVAMP3= 21.15 ± 2.12 , GFP-Rabin8= 50.49 ± 4.21). All the above graphs show mean \pm s.e.m from three independent experiments (ns, no significant *, $p < 0.05$; **, $p < 0.01$; ***, $p < 0.001$ by one-way ANOVA with Tukey's multiple comparison post test). Scale bar=10 μ m

Table S1. Data of High content subfamily-wide screening of 41 Rab GTPases overexpressed in CAD cells. Relative percentage of acceptor cells containing DID labeled vesicles that transferred from donor cells. Data were normalized to control conditions. Values of score when applying two thresholds (95% and 105%) to data and sum of 4 experiments.

	Exp1	Exp2	Exp3	Exp4		Exp1	Exp2	Exp3	Exp4		Sum
MyoX	107.93%	109.37%	112.50%	110.39%	MyoX	1	1	1	1		4
GFP-v	100.00%	100.00%	100.00%	100.00%	GFP-v	0	0	0	0		0
VASP	92.13%	88.02%	81.51%	93.09%	VASP	-1	-1	-1	-1		-4
1A	109.17%	94.51%	84.88%	55.33%	1A	1	-1	-1	-1		-2
2A	110.05%	86.38%	80.39%	103.71%	2A	1	-1	-1	0		-1
3A	112.08%	80.95%	95.25%	101.51%	3A	1	-1	0	0		0
4A	115.66%	91.82%	95.29%	98.63%	4A	1	-1	0	0		0
5A	104.66%	76.50%	87.56%	106.94%	5A	0	-1	-1	1		-1
6A	106.59%	80.34%	86.77%	100.27%	6A	1	-1	-1	0		-1
7	101.78%	84.04%	90.57%	111.21%	7	0	-1	-1	1		-1
8A	107.01%	108.08%	105.63%	128.07%	8A	1	1	1	1		4
9A	115.70%	100.75%	89.89%	97.69%	9A	1	0	-1	0		0
10	105.29%	86.96%	85.37%	92.61%	10	1	-1	-1	-1		-2
11A	117.84%	109.95%	113.80%	113.33%	11A	1	1	1	1		4
12	109.42%	77.45%	87.59%	106.15%	12	1	-1	-1	1		0
13	111.35%	87.43%	89.02%	103.90%	13	1	-1	-1	0		-1
14	110.73%	93.12%	95.37%	95.85%	14	1	-1	0	0		0
15	97.54%	92.79%	98.66%	107.64%	15	0	-1	0	1		0
17	96.41%	96.10%	94.23%	109.72%	17	0	0	-1	1		0
18	86.38%	104.31%	98.22%	105.74%	18	-1	0	0	1		0
19	98.54%	100.14%	96.50%	107.10%	19	0	0	0	1		1
20	98.16%	92.85%	98.85%	95.93%	20	0	-1	0	0		-1
21	100.56%	104.45%	93.08%	99.04%	21	0	0	-1	0		-1
22A	96.99%	102.68%	88.51%	105.15%	22A	0	0	-1	1		0
23	91.60%	103.93%	99.42%	105.98%	23	-1	0	0	1		0
24	103.02%	102.75%	94.73%	95.79%	24	0	0	-1	0		-1
25	107.50%	96.46%	96.04%	91.11%	25	1	0	0	-1		0
26	108.86%	98.59%	79.29%	94.74%	26	1	0	-1	-1		-1
27A	109.41%	99.98%	94.92%	104.40%	27A	1	0	-1	0		0
28	112.98%	96.42%	95.79%	110.77%	28	1	0	0	1		2
29/7L1	108.33%	107.84%	88.99%	111.77%	29/7L1	1	1	-1	1		2
30	95.64%	104.62%	104.67%	95.82%	30	0	0	0	0		0
32	99.32%	98.44%	92.22%	96.71%	32	0	0	-1	0		-1
33A	100.09%	107.99%	117.41%	94.90%	33A	0	1	1	-1		1
34	102.04%	106.63%	80.69%	96.67%	34	0	1	-1	0		0
35	116.37%	106.11%	116.65%	108.16%	35	1	1	1	1		4
36	89.69%	105.77%	91.37%	97.60%	36	-1	1	-1	0		-1
37	96.08%	96.22%	90.52%	99.32%	37	0	0	-1	0		-1
38	88.35%	101.39%	110.89%	100.96%	38	-1	0	1	0		0
39A	91.44%	91.82%	88.58%	92.65%	39A	-1	-1	-1	-1		-4
40A	79.21%	92.13%	90.86%	92.26%	40A	-1	-1	-1	-1		-4
41/43	95.75%	107.68%	74.22%	102.27%	41/43	0	1	-1	0		0
42/7B	106.34%	100.20%	71.50%	95.93%	42/7B	1	0	-1	0		0
43/42	86.40%	105.30%	91.29%	100.40%	43/42	-1	1	-1	0		-1

Table S2. Data showing average percentage of TNT connected cells. Cells transfected with the plasmids as mentioned and the corresponding average of percentage of TNT connected cells showing \pm s.e.m.

Plasmids	Average Percentage of TNT connected cells
GFP-vector	57.44 \pm 2.50
Rab11a-WT	76.68 \pm 4.13
Rab11a-Q70L	92.25 \pm 3.01
Rab11a-S25N	65.70 \pm 3.95
Sh CTL	56.71 \pm 3.41
Sh Rab11a	40.81 \pm 0.99
Sh Rab11a/GFP-Rab11a	59.34 \pm 3.30
GFP-vector	51.32 \pm 1.9
Rab8a-WT	76.4 \pm 2.06
Rab8a-Q67L	79.17 \pm 5.07
Rab8a-T22N	53.47 \pm 1.94
Sh CTL	56.71 \pm 3.41
Sh Rab8a	46.15 \pm 4.238
Sh Rab8a/GFP-Rab8a	69.07 \pm 13.14
Sh CTL	52.35 \pm 3.40
Sh Rab11a	39.94 \pm 1.32
Sh Rab11a/GFP-Rab8a	61.43 \pm 1.228
Sh CTL	52.35 \pm 3.40
Sh Rab8a	40.98 \pm 4.86
Sh Rab8a/GFP-Rab11a	42.78 \pm 2.403
GFP-Vector	44.47 \pm 6.79
GFP-GRAB	56.18 \pm 10.64
ShCTL/GFP	38.86 \pm 1.71
shRab8/GFP	30.38 \pm 0.38
shRab8/GRAB	49.36 \pm 2.36
H2O	68.92 \pm 2.876
PMQ	44.17 \pm 5.077
GFP-vector	56.56 \pm 4.94
VAMP3	71.45 \pm 6.07
Sh CTL	55.04 \pm 1.050
Sh VAMP3	44.97 \pm 1.463
Sh VAMP3/GFP-VAMP3	69.84 \pm 1.017
Sh CTL	56.65 \pm 2.04
Sh VAMP3	46.18 \pm 2.078
Sh VAMP3/GFP-Rab8a	51.45 \pm 4.92
Sh CTL	56.65 \pm 2.04
Sh VAMP3	46.18 \pm 2.07
Sh VAMP3/GFP-Rab11a	49.46 \pm 2.22